HATSOPOULOS MICROFLUIDS LABORATORY
Department of Mechanical Engineering, Massachusetts Institute of Technology

Drop Formation and Breakup of Low Viscosity Elastic Fluids: Effects of Molecular Weight and Concentration

V. Tirtaatmadja, Gareth H. McKinley, and Justin J. Cooper-White

January 2006
HML Report Number 06-P-03

HML@MIT
http://web.mit.edu/fluids

Drop Formation and Breakup of Low Viscosity Elastic Fluids: Effects of Molecular Weight and Concentration

V. Tirtaatmadja[1], G.H. McKinley[2] and J.J. Cooper-White[1*]

[1]Particulate Fluids Processing Centre, Department of Chemical and Biomolecular Engineering, The University of Melbourne, Parkville 3010, Australia

[2] Hatsopoulos Microfluids Laboratory, Department of Mechanical Engineering, Massachusetts Institute of Technology, Cambridge, Massachusetts, MA 02139, USA

[*] *Author to whom correspondence should be addressed. Division of Chemical Engineering, The University of Queensland, St. Lucia, 4072 Email: j.cooperwhite@uq.edu.au*

Abstract

The dynamics of drop formation and pinch-off have been investigated for a series of low viscosity elastic fluids possessing similar shear viscosities, but differing substantially in elastic properties. On initial approach to the pinch region, the viscoelastic fluids all exhibit the same global necking behaviour that is observed for a Newtonian fluid of equivalent shear viscosity. For these low viscosity dilute polymer solutions, inertial and capillary forces form the dominant balance in this potential flow regime, with the viscous force being negligible. The approach to the pinch point, which corresponds to the point of rupture for a Newtonian fluid, is extremely rapid in such solutions, with the sudden increase in curvature producing very large extension rates at this location. In this region the polymer molecules are significantly extended, causing a localised increase in the elastic stresses, which grow to balance the capillary pressure. This prevents the necked fluid from breaking off, as would occur in the equivalent Newtonian fluid. Alternatively, a cylindrical filament forms in which elastic stresses and capillary pressure balance, and the radius decreases exponentially with time. A (0+1)-dimensional FENE dumbbell theory incorporating inertial, capillary and elastic stresses is able to capture the basic features of the experimental observations. Before the

critical 'pinch time' t_p, an inertial-capillary balance leads to the expected 2/3-power scaling of the minimum radius with time, $R_{\min} \sim (t_p - t)^{2/3}$. However, the diverging deformation rate results in large molecular deformations and rapid crossover to an elasto-capillary balance for times $t > t_p$. In this region the filament radius decreases exponentially with time $R_{\min} \sim \exp[(t_p - t)/\lambda_1]$ where λ_1 is the characteristic time constant of the polymer molecules. Measurements of the relaxation times of PEO solutions of varying concentrations and molecular weights obtained from high speed imaging of the rate of change of filament radius are significantly higher than the relaxation times estimated from Rouse-Zimm theory, even though the solutions are within the dilute concentration region as determined using intrinsic viscosity measurements. The effective relaxation times exhibit the expected scaling with molecular weight but with an additional dependence on the concentration of the polymer in solution. This is consistent with the expectation that the polymer molecules are in fact highly extended during the approach to the pinch region (i.e. prior to the elasto-capillary filament thinning regime) and subsequently as the filament is formed they are further extended by filament stretching at a constant rate until full extension of the polymer coil is achieved. In this highly-extended state, inter-molecular interactions become significant producing relaxation times far above theoretical predictions for dilute polymer solutions under equilibrium conditions.

I INTRODUCTION

The dynamical mechanisms of drop formation and fluid rupture from a nozzle under the influence of gravity alone (i.e. dripping regime) or due to the application of external forces (i.e. jetting regime) have been studied since the mid 19th century[1-3]. Numerous researchers have since made significant experimental and numerical contributions to the field, providing insight into the discrete behaviour of Newtonian fluids on approach to and past the "pinch" region during dripping and jetting[4-7]. In particular, the effects of viscosity[7-13] and surface tension[8, 14] on breakup dynamics, and subsequent formation of drops have been thoroughly investigated. Simplified formulations of the Navier-Stokes equations for incompressible flow with a free surface have been produced in a number of studies in an effort to understand the physical mechanisms governing drop formation[15-18]. The effects of fluid flow within and surrounding[19] the forming drop have also been considered. Numerical algorithms permitting solutions of the complete Navier-Stokes equations describing drop formation have also recently been developed[12, 20]. The finite element calculations of Wilkes *et al*.[12] were able to capture both the gross features of the drop formation, including the limiting length of a drop at breakup, and the fine scale features such as secondary threads that form from the main thread at certain fluid conditions. Numerical methods can now provide reasonable prediction of resultant drop length and time scales for Newtonian fluids with constant material properties; i.e. constant density, viscosity, surface tension (see for example Chen *et al*.[21]).

Many materials of commercial interest however may exhibit non-Newtonian fluid properties. Current interest in this field is in understanding the effects of non-Newtonian fluid properties, including shear thinning and elasticity, on liquid bridge breakup and drop formation and breakup. A number of recent studies have focused on the use of 'liquid filament rheometers' or 'capillary breakup rheometers' as a means to investigate the dynamics of complex fluids

undergoing extensional flows that are driven by the presence of a free-surface[22]. Liang and Mackley[23] studied the effects of varying polymer concentration on the time to breakup; and the results are consistent with the predictions of a one-dimensional theory for capillary-thinning of a liquid filament containing a multimode suspension of finitely extensible nonlinear elastic (FENE) dumbbells[24]. However the particular range of concentrations studied (which were in the semi-dilute regime) and the molecular polydispersity of the polyisobutylene polymer precluded a quantitative comparison of the measurement with predictions from polymer kinetic theory. McKinley and Tripathi[25] and Anna and McKinley[26] used a series of model monodisperse dilute polymer solutions to show that the relaxation time extracted from capillary-thinning experiments exhibits the expected scaling with molecular weight. These ideal elastic fluids consist of dilute concentrations of polymer below the critical coil overlap concentration (denoted c^*) and utilize a viscous oligomeric oil as the solvent. Since kinetic theory for dilute polymer solutions predicts that both the polymer relaxation time and the polymer contribution to the viscosity scale with the solvent viscosity[27], the elastic stresses in such fluids are amplified and inertial effects are minimized. However it is not possible to relate the results of these studies to measurements of capillary thinning and drop pinch-off in lower viscosity fluids for which inertial effects cannot be ignored.

Several recent experimental studies of low viscosity elastic solutions in the capillary-thinning device, such as those of Stelter *et al.*[28, 29] and Bazilevskii *et al.*[30], have provided much needed insight into the dynamics of breakup of thin polymeric filaments. In contrast to the very viscous fluids studied by Anna and McKinley[26], an initial high rate of filament thinning was observed in the lower viscosity solutions and was attributed to a balance between inertial and capillary effects, with elastic stress being unimportant in this region[30]. This is followed by a

slower filament thinning region, during which capillary pressure is balanced by fluid elastic stresses. In this region, the filament diameter shows an exponential decrease with time, with the exponential thinning rate being inversely proportional to the characteristic relaxation time of the solutions in agreement with the analysis of Entov and Hinch[24]. Finally when the polymer becomes fully extended and the viscoelastic contribution to the extensional viscosity saturates, the exponential rate of filament thinning can no longer be sustained. In this region, a linear rate of filament reduction with time is again encountered until breakup occurs. Both Stelter *et al*.[29] and Bazilevskii *et al.*[30]found that the characteristic relaxation times obtained from the exponential rates of filament decrease are dependent on polymer concentration, even though the Rouse-Zimm theory predicts that in the dilute region the relaxation time should be dependent only on molecular weight, but not on concentration. Moreover, Bazilevskii *et al*.[30] reported that the relaxation times obtained experimentally from the exponential rate of radius reduction for aqueous polymer solutions are generally higher than the expected value, while the values for the higher viscosity solutions in glycerol and glycerol-water mixtures (with solvent viscosity of the order of 1 Pa.s) are much lower than the expected value, although still dependent on concentration. In contrast, Anna and McKinley[26] found that the relaxation times obtained from the exponential filament thinning rates in a capillary thinning device for their constant high viscosity, elastic solutions (of polystyrene in an oligomeric styrene solution of viscosity of approximately 23 Pa.s) agreed well (to within experimental error) with the longest relaxation times obtained from fitting a Zimm spectrum to small amplitude oscillatory shear data. It is worth noting that scaling with concentration was not investigated in this study.

As an alternative approach to capillary thinning, Schummer and Tebel[31] some time ago studied the effects of fluid elasticity on the breakup of liquid jets into drops under forced

disturbances. They suggested that by periodically forcing the jet it may be possible to quantify the effects of extensional stresses in a necking fluid thread formed between drops. However, the need for high speed photography and subsequent image analysis inhibited widespread application of the technique until recently. Li and Fontelos[32] and Clasen *et al*.[33] used numerical simulations to study the dynamics of the beads-on-string structure of forced liquid jets of an Oldroyd-B fluid. Clasen *et al*.[33] found good agreement of their 1D numerical simulation with experimental results for high viscosity viscoelastic fluids. Amarouchene *et al*.[34] and Cooper-White *et al*.[35] studied drop formation from a nozzle under gravity of low viscosity, elastic fluids, while Mun *et al*.[36], Christanti and Walker[37] studied the drop breakup under forced jetting. Cooper-White *et al*.[35] and Christanti and Walker[37] studied dilute, low viscosity polymer solutions of varying molecular weights and found that the relaxation times obtained from measurements of the rates of thinning of the primary filament were much larger than the Zimm relaxation times calculated from the known concentration and molecular weight of the polymer in agreement with Bazilevskii *et al.*[30] Cooper-White *et al*.[35] also found the final length of the filament at detachment and the time of break-off was proportional to the relaxation time of the solutions. Amarouchene *et al*.[34] investigated two high molecular weight polymers in aqueous solutions over a range of concentrations and found the effective relaxation times obtained from the rates of filament thinning to be dependent on the concentrations of the polymer in solution, even in the dilute regime. The authors did not give any information on the shear viscosity of their solutions, which were most likely to show significant shear-thinning characteristics, due to the differing concentrations and polydispersity of the high molecular weight polymers studied. The authors also did not provide values of the relaxation time of the solutions expected from molecular theory. However, a significant result of the work of Amarouchene *et al*.[34] is the realisation that as the drop approaches the Newtonian pinch region (as indicated by a rapid reduction in

the minimum drop radius), the fluid exceeds a critical extension rate prior to the formation of a viscoelastic filament connecting the droplet to the fluid above. This critical extension rate, which can be determined from the rapid change in the slope of the radius-time plot, is much higher than the rate of subsequent filament elongation and is the dominant source of polymer extension, as also pointed out by Cooper-White *et al*.[35] It is this rapid increase in the extension rate immediately prior to the pinch point which causes the stretching of the polymer molecules in solution and the large increase in the polymer elastic stress. This elastic stress then resists the capillary pressure, inhibiting the primary drop from pinching-off. No simple model currently exists to describe this behaviour of low viscosity viscoelastic fluids in the drop formation and breakup process.

In this paper we extend our previous work into drop formation dynamics of constant low viscosity, elastic fluids by systematically probing the effects of polymer molecular weight and concentration down to the ultradilute regimes. Furthermore, we present a simple one-dimensional model that captures the dynamics of the pinching process for low viscosity elastic solutions in which inertial effects are dominant prior to the emergence of fluid elastic stress to balance the capillary pressure. In this study, as in our previous work, we have used the same nozzle for all experiments, the liquid flowrate is kept constant, and the shear viscosity and equilibrium surface tension are adjusted to be approximately equal and constant for all solutions. The variation in the minimum drop radius is measured using high speed digital imaging analysis and compared to the predictions obtained from a one-dimensional inertio-elastic pinch model. The relaxation times obtained from the rate of filament radius reduction are compared to the theoretical values of the longest Zimm relaxation time computed from intrinsic viscosity measurements. The mechanics of the drop evolution up to

the point of breakup are discussed for solutions with differing levels of elasticity, and the physical mechanism that helps inhibit the capillary breakup process is described.

II EXPERIMENTAL METHOD

A Test solutions and their preparation

The low-viscosity elastic fluids tested in this work are dilute solutions of polyethylene oxide (PEO) (supplied by Aldrich Chemical Co.), with molecular weights ranging from 3×10^5 to 5×10^6 g/mol, in glycerol and water mixtures. The commercial PEO samples are known to be polydisperse; for example, the PEO of molecular weight 1×10^6 g/mol has been determined using size exclusion chromatography technique to have the ratio $M_w / M_n \sim 1.8$[38], and other molecular weight samples are thus expected to have similar polydispersity. In this work, the polymer concentrations were varied, while keeping below the coil overlap concentration, c^*. These solutions were all prepared so that the shear viscosity, which was constant in all cases between shear rates of 1 and 100 s^{-1}, was approximately $\eta = 6\times10^{-3}$ Pa.s and the equilibrium surface tension was approximately $\sigma = 60\times10^{-3}$ N/m at 21°C.

In preparing the solutions, Milli-Q water was first warmed to about 40°C, followed by addition of polymer and constant stirring for 2 hours thereafter. The solutions were then mixed by gently rolling for another 24 hours before the addition of glycerol, and then rolled for a further 24 hours prior to use in the experiments. Most solutions were prepared by this method, with the exception of the series of solutions containing PEO of molecular weight 1×10^6 g/mol of varying polymer concentrations in a solvent of 45wt% glycerol/55wt% water, which were prepared by dilution of the original 0.1 wt% 1×10^6 g/mol PEO solution to the required concentrations.

The shear viscosity of the solutions and the solvents was measured using a Carrimed CSL-100 controlled-stress rheometer (with a conical fixture of 60-mm diameter and 0.04-radian cone angle). These properties together with the fluid compositions are provided in Table 1 for a series of PEO solutions with varying molecular weight at approximately constant dimensionless concentration $c/c^* \sim 0.5$, and in Table 2 for another series of PEO solutions of $M_w = 1\times10^6$ g/mol with varying concentrations. In addition to the solutions shown in Tables 1 and 2, other solutions of PEO with molecular weight up to 5×10^6 g/mol and various concentrations were also prepared and used in this study.

The measured shear viscosity of the solutions used in this study ranges between 4.4×10^{-3} and 8.1×10^{-3} Pa.s. However, the elastic properties of the solutions, such as the storage modulus G', could not be measured even with the most sensitive rheometer available to us (Rheometric Scientific ARES). Hence in an attempt to quantify the viscoelasticity of the solutions, the extensional viscosity of the various molecular weight PEO solutions, at concentration $c/c^* \sim 0.5$ in a solvent of 50wt% glycerol, was measured using a Rheometric RFX opposing-jet rheometer. Results for solutions of similar c/c^* are not presented here but are shown in Figure 4 of Cooper-White *et al.*[35] for molecular weights up to 1×10^6 g/mol, together with additional results for the 2×10^6 and 5×10^6 g/mol solutions. The data indicate that the ratio of the apparent extensional viscosity to shear viscosity (i.e. the Trouton ratio, $Tr = \eta_e / \eta_0$) increases with increasing molecular weight of PEO at equivalent apparent extension rates. The critical extension rates at which deviation from the value $Tr = 3$ (expected for a Newtonian fluid) occurred were found to decrease with increasing polymer molecular weight. For solutions with varying concentration, the scaled extensional viscosity of the 1×10^6 g/mol PEO solutions display similar characteristics to those shown for solutions

of 3×10^5 g/mol PEO in water/glycerol given in Crooks *et al*.[39] In this latter case, the Trouton ratio also increases with increasing polymer concentration at the same apparent extension rate, but the critical extension rate at which deviation from a value of $Tr = 3$ occurred was the same for all concentrations.

B Image capture and measurement of drop formation dynamics

The drop formation study was carried out with the fluid exiting from a nozzle of 2.0 mm inner diameter and 4.0 mm outer diameter. The fluid was fed from a syringe pump at a rate of 73.8 ml/min. This is the same rate as that used by Cooper-White *et al*.[35] in their drop formation study of similar fluids. Several drops of fluid were allowed to form to ensure a constant liquid flowrate prior to the images of the drop being taken for analysis. A sequence of images of the drop during its formation, subsequent approach to pinching and elongation of the necked fluid into a thin filament connecting the primary drop to the upper reservoir of fluid (in the case of polymer solutions with high elasticity) were taken using a high speed video camera (Phantom V, Vision Research). The camera can capture up to 1000 frames per second at 1024 by 1024 pixels, or capture higher frame rates at lower resolutions. To investigate the dynamics of drop formation, the minimum diameter of the fluid thread as it exits the nozzle is followed and measured until the final break-off occurs, either in the secondary thread between the primary drop and the filament, or in the secondary thread between the filament and the remaining fluid attached to the nozzle. The minimum measurable diameter is equivalent to between 8 to 12 microns, i.e. 2 to 3 pixels using the given experimental configuration.

C Intrinsic viscosity and Zimm relaxation time

The intrinsic viscosity of the PEO solutions at various molecular weight in an aqueous solvent containing 36% glycerol was measured using a capillary viscometer (Schott Grate Ubbelohde type no. 53110), with automatic diluter. The data are plotted as a function of molecular weight in Figure 1. Also shown in the figure are the results obtained by other researchers, both in this laboratory[38, 39] and elsewhere[37, 40], in water and glycerol/water mixtures. The molecular weights of the PEO span a range from $8\times10^3 \le M_w \le 5\times10^6$ g/mol. All the data agree well with each other within experimental errors, although there are some systematic variations with solvent composition. A linear regression analysis has been used to obtain a line of best fit to all the data, giving a composite Mark-Houwink-Sakurada (MHS) equation for the intrinsic viscosity $[\eta]$ of the PEO solutions:

$$[\eta] = 0.072 M_w^{0.65} \tag{1}$$

with $[\eta]$ in units of cm^3/g. Also shown for comparison is the line for a narrow molecular-weight distribution PEO up to $M_w = 3\times10^4$ g/mol in water, obtained from the Polymer Handbook. The MHS exponent of $a \approx 0.65$ obtained in our composite curve is similar to the tabulated value from the Polymer Handbook[41] of $a = 0.67$. The Zimm theory for dilute solutions of polymer coils in a solvent incorporating hydrodynamic interactions gives the scaling $[\eta] \sim M_w^{3\nu-1}$ for long chains. Here ν is the exponent characterising the scaling of the equilibrium radius of gyration of the chain with molecular weight, i.e. $Rg \sim M_w^{\nu}$. The limiting values of ν = 0.5 and ν = 0.6 correspond to a theta solvent and a good solvent respectively[42]. The regression of our data gives ν = 0.55 indicating that both water and mixtures of glycerol and water over the range tested are relatively good solvents for PEO, as expected.

The critical overlap concentration c^* is defined as the concentration at which the polymer coils start to overlap with each other. Below c^* the solution is considered to be in the dilute regime and the viscoelastic properties of the solution are governed by the behavior of a single polymer molecule[27]. In order to determine c^* of the PEO solutions studied, we have used the classification of Flory for flexible polymer solutions, where

$$c^* = 1/[\eta] \tag{2}$$

Alternatively c^* can be determined as the concentration at which the product of the number density of polymer coils and the volume pervaded by a single coil is equal to unity. The volume of the coil has to be calculated from the radius of gyration, which can be estimated from the known properties of PEO, such as the characteristic ratio C_∞ and the excluded volume exponent v. These values are consistent to within 20% of the values calculated from Equation (2). Finally, Graessley[43] introduced a somewhat modified definition of $c^* = 0.77/[\eta]$, resulting in the critical overlap concentration of the solutions being lower than those obtained above by a further factor of 23%. In the remainder of this paper, the overlap concentrations of the PEO solutions reported are those calculated from Equation (2), using the intrinsic viscosities determined from Equation (1).

For a polymer chain in a good solvent, the longest relaxation time in the Zimm theory can be approximated by:

$$\lambda_Z \cong \frac{1}{\zeta(3\nu)} \frac{[\eta] M_w \eta_s}{N_A k_B T} \tag{3}$$

where η_s is the solvent viscosity, N_A the Avogadro's number, k_B the Boltzmann constant and T the temperature. The precise value of the numerical front factor in Equation (3) must be determined from a detailed eigenvalue calculation[44]. In the limit of dominant hydrodynamic

interactions this value is $1/(2.369) = 0.422$. For other values of the solvent quality the front factor can be approximated by $1/\zeta(3\nu)$ where $\zeta(3\nu) = \sum_{i=1}^{\infty} 1/i^{3\nu}$. For $\nu = 0.55$ the front factor is thus $1/\zeta(1.65) \simeq 0.463$. Using this equation together with the values of intrinsic viscosity, the longest Zimm relaxation time can be calculated from the polymer molecular weight and solvent viscosity (noting that the intrinsic viscosity is assumed to be a function only of the molecular weight for dilute solutions). The values of λ_Z for a series of PEO solutions of varying molecular weight at fixed dimensionless concentration $c/c^* \sim 0.5$ in a solvent of 36wt% glycerol are given in Table 1, and the values for a series of PEO solutions of M_w = 1×10^6 g/mol over a range of polymer concentrations in a solvent of 45wt% glycerol are given in Table 2.

Finite concentration effects are also expected to further modify Equation (3). A simple mean field approach would suggest that as a first approximation the effective viscosity of the solvent is replaced by the shear viscosity η of the solution. This is also consistent with writing the viscosity of the dilute solutions as a Taylor series of the form

$$\eta = \eta_s \{1 + [\eta]c + O(c^2)\} \qquad (4)$$

and evaluating the intrinsic viscosity using the expression determined from the data in Figure 1. From Table 1, variations of up to 75% may thus be anticipated for the high concentration solutions with the deviation decreasing at lower concentrations. The systematic deviations of the relaxation time that we determined from the experiments in section 4 are beyond those obtained by combining equations (3) and (4).

The relaxation times for these dilute aqueous solutions span the range $5\times10^{-5}\,\mathrm{s} \le \lambda_Z \le 7\times10^{-3}\,\mathrm{s}$. Although these values are small, viscoelastic effects may still be important due to the large deformation rates that occur close to drop pinch-off, as we show below.

D Dynamic surface tension

The dynamic surface tension (DST) data for the PEO solutions with varying molecular weights are given in Cooper-White *et al*.[35] and Crooks *et al*.[39] The data show differences at short time, with the higher molecular weight PEO taking longer time to approach equilibrium than the more mobile polymers[35, 39]. However, the various PEO solutions attained the same equilibrium value of $\sigma \simeq 62\times10^{-3}$ N/m. As the drop formation and subsequent breakup process occurs within time scale of 0.1 s or less, it is this "dynamic" surface tension of the solutions which is expected to be the relevant driving factor in this capillary thinning process.

The dynamic surface tension also varies with polymer concentration. Data for the solutions of 1×10^6 g/mol PEO at various concentrations, measured using a Maximum Bubble Pressure Tensiometer (Kruss BP2), are shown in Figure 2. The results indicate that the DST value is lower the higher the polymer concentration, with the solutions of lower bulk concentrations taking longer times to attain equilibrium surface tension. Also shown in the figure (by hollow symbols) are the variations in the DST for three solutions of varying concentrations (of the same molecular weight PEO) and with 0.4wt% 2-butanol added. The data show that with the addition of 2-butanol, the surface tension is lowered to near the equilibrium value at very short times. The addition of small quantities of 2-butanol has also been used by others[39, 45] to reduce the surface tension of various PEO solutions at short time. It will be shown later that the variation in the dynamic surface tension at short times (of the order of 10×10^{-3} N/m) is

insufficient to account for the difference in the drop breakup dynamics observed. This is demonstrated by the similar filament thinning behaviour observed for the solutions with and without 2-butanol added (cf. Figure 9 below).

III A MODEL FOR INERTIO-ELASTIC PINCHING

Recent experiments in low-viscosity dilute polymer solutions exiting a nozzle and undergoing breakup under the effect of gravity[35] have shown that similar dynamical phenomena are observed in a continuous jet undergoing breakup[36], and under forced disturbances of a known wavelength[37]. The resulting dynamics are always found to vary strongly with the molecular weight of the dissolved macromolecules, and differ significantly from those observed in a Newtonian fluid. In this section we present a simple one-dimensional model that captures the general features of the dynamics of the drop breakup from a nozzle for a viscoelastic fluid.

In Figure 3 we show a sequence of images of the drop formation process for two representative cases; a Newtonian glycerol-water mixture and a viscoelastic solution of 0.1 wt% PEO (M_w = 1×10^6 g/mol), with the solutions having an identical shear viscosity ($\eta = 6\times10^{-3}$ Pa.s) and similar equilibrium surface tensions of $\sigma = 70\times10^{-3}$ N/m and $\sigma = 62\times10^{-3}$ N/m respectively. The initial stages of the pinching process are very similar for both fluids. However as the necked region connecting the primary drop to the nozzle forms, it is clear that elastic effects lead to systematic differences in the dynamics of breakup, resulting in the classic 'bead-on-a-string' morphology. We note that in a previous study[35] it was found that two Newtonian fluids, a glycerol-water mixture and a solution containing PEO of M_w = 8×10^3 g/mol (with an estimated Zimm relaxation time of the order of 1×10^{-7} s), whose surface

tension values also differed from each other by approximately 8×10^{-3} N/m, exhibited no significant difference in the drop breakup dynamics. Hence it can be concluded that the small difference in surface tension of 8×10^{-3} N/m is insufficient to impart the observed difference in the drop breakup dynamics shown in Figure 3.

In Figure 3, the times indicated are the shifted time ($t - t_p$) in milliseconds, relative to the critical pinch-off time t_p. Note that the critical pinch-off time t_p of the elastic solutions given here is equivalent to the difference between the detachment time and the lag time ($t_d - t_l$) defined in Cooper-White *et al.*[35] and is obtained during post-processing of the images by horizontally shifting the curves of the minimum radius of the necking fluid drop $R_{min}(t)$ along the time axis until they coincide with the Newtonian fluid curve (see Figures 7(a) and 9 below for examples). For $(t - t_p) < 0$, elastic effects are relatively unimportant; however for $(t - t_p) > 0$, the elastic stress is the dominant term resisting pinch-off, and the necked fluid is formed into a long thin thread connecting the primary drop to the upper reservoir of fluid which remains attached to the exit nozzle. For the viscoelastic solution, this initial necking process is identical to the Newtonian fluid until approximately 1 or 2 ms before the critical pinch time t_p.

It is also clear from the images shown in Figure 3 that as the critical pinch time t_p is approached, this viscoelastic fluid filament becomes increasingly long and slender. As a first approximation, it is therefore appropriate to develop a simple one-dimensional model of the time-varying extensional flow that arises when the fluid drop exits the nozzle, approaches the pinch region, and thereafter forms the thin filament of fluid connecting the primary drop to the upper reservoir of fluid. Dimensional analysis suggests that the important dimensionless

groups characterizing this necking process are the Ohnesorge number $Oh = \eta_0 \Big/ \sqrt{\rho \sigma R_0}$ and the intrinsic Deborah number $De_0 = \lambda_Z \Big/ \sqrt{\rho R_0^3 / \sigma}$, formed from the ratio of the viscoelastic relaxation time and the characteristic Rayleigh breakup time. The values of Oh and De_0 for the PEO solutions are also given in Tables 1 and 2, where we have used the outer radius of the nozzle (R_0=2 mm) as the characteristic length scale since the pendant drop wets the annular rim, and ρ and σ are the density and surface tension of the fluid respectively. For the low viscosity polymer solutions used in this work and in other recent experiments[34, 35, 37], we may have $De_0 \sim O(1)$ (depending on the molecular weight of the dissolved polymer) but also $Oh << 1$ such that viscous effects of the suspending solvent are always negligible during both the early and late stages of the pinch-off process. We are therefore interested here in the seldom-explored limit of potential flows of elastic liquids or *inviscid elastic flow*. Funada and Joseph[46] have recently studied the linear stability of viscoelastic jets when the flow field is approximated by a potential function (corresponding to inviscid flow). They show that the results are very close to those obtained by exact computation using the Navier-Stokes equation and the potential flow analysis has the additional benefit of being simple enough to enable analytic progress to be made.

Entov and Hinch[24] carried out an analysis for the capillary-induced necking of highly viscous polymeric fluids (corresponding to $Oh >> 1$) using the FENE-P dumbbell model. As the filament radius decreased, the balance of forces evolved from a visco-capillary balance (corresponding to a linear decrease of the radius with time that scales with the capillary velocity $v_{cap} \sim \sigma / \eta_0$) to an elasto-capillary balance in which the capillary pressure driving the necking process is resisted by the elastic stress in the highly elongated dumbbells. In this intermediate regime, the theory and experiments on highly viscous ideal elastic polymer

solutions[22, 26] show that the radius of the slender filament decreases exponentially with time until the finite extensibility of the molecules becomes important. In this final region, the extensional viscosity $\eta_E(\dot{\varepsilon})$ is high, due to the highly stretched molecules, and almost constant; the necking then becomes linear in time once more but with a characteristic velocity $v \sim \sigma / \eta_E$.

Recent experimental studies in dilute polymer solutions with $Oh << 1$ have shown that following the formation of a slender thread of the type shown in Figure 3 for the 0.1wt% PEO solution, there is an analogous crossover to an exponential rate of necking[29, 30, 34, 37]. Measurements of the necking rate have been used to extract estimates of the relaxation time for the polymer chains. The initial necking however is not linear in time due to the low viscosity of the fluids and instead appears to be inertially-dominated. Here we seek a simple model that is capable of capturing the essential features of this cross-over from inertio-capillary necking to an elasto-capillary balance.

We consider an axially-uniform cylindrical thread of fluid under the action of capillary, inertial and elastic stresses. Following the notation of Eggers[47] we refer to this as a *(0+1) dimensional* (spatial + temporal) approximation, or more compactly a 'zero-dimensional model'. Such a description cannot be expected to provide quantitative agreement with experiments or full numerical simulations because it neglects axial variations in the structure of the thread. In particular, for inviscid irrotational flows it has been shown that the simplified one-dimensional Euler equations exhibit a singularity before the point of breakup is reached[48]. Numerical simulations [49, 50] show that in fact the free-surface of the droplet close to the singularity overturns.

The analysis below may thus be considered a simplified or 'toy' model that captures the key features of the dynamical process and the cross-over from an inertio-capillary balance to an elasto-capillary balance. Such a description has not been presented to date. It is also worth noting that there now exists substantial evidence for both viscous Newtonian fluids[26] and viscoelastic fluids with $Oh >> 1$[24, 26, 28] that such a simplified model description provides the correct scaling of the evolution in the radial profile with time. In the case of a viscous Newtonian fluid ($Oh >> 1$, $De_0 = 0$), the value of the prefactor can be obtained from the similarity solution of Papageorgiou[17]. Recent numerical simulations[51] of the formation of a beads-on-a-string structure for low viscosity viscoelastic fluids ($Oh \sim O(1)$, $De \sim 0(1)$) suggest that a (0+1)-dimensional force balance also results in the correct exponential decay in the filament radius for this class of fluids and incurs a maximum error in the prefactor of $2^{-1/3} \approx 0.793$. Such a (0+1)-dimensional approximation thus seems to be a worthwhile place to start.

The general form of the force balance for slender viscoelastic threads has been discussed and derived elsewhere[52]. An axial force balance coupled with a radial force balance to eliminate the unknown pressure in the thread results in an equation of the general form

$$\tfrac{1}{2}\rho\dot{R}(t)^2 \sim \frac{F(t)}{\pi R^2(t)} - \frac{\sigma}{R(t)} - 3\eta_s\left(\frac{-2\dot{R}(t)}{R(t)}\right) - \Delta\tau_p(t) \qquad (5)$$

The time-evolving polymeric stress difference in the filament is denoted generically by $\Delta\tau_p(t) = \Delta\tau_p = [\tau_{pzz}(t) - \tau_{prr}(t)]$ and $F(t)$ is the unknown tensile force in the column. The local (time-varying) radial rate of necking is $\dot{\varepsilon}(t) = -2\dot{R}(t)/R(t)$.

In the present (0+1) model of the pinch-off process, the necking filament is connected to the primary drop (which is accelerating under the action of a gravitational body force) and to the remaining fluid held in the reservoir attached to the upper *nozzle*. These upper and lower regions are in a quasi-static balance between capillarity and gravity and are connected by an axially-uniform cylindrical filament. Following McKinley & Tripathi[25] we assume that as a result the appropriate boundary conditions on the unknown tensile force *F(t)* is that $F(t) \to 2\pi\sigma R(t)$. The upper and lower fluid reservoirs essentially serve to relieve the no-slip boundary condition on the radial velocity of the fluid column and promote a uniaxial extensional flow. A more complete (1+1)-dimensional analysis such as that described by Wagner et al.[48] is needed to determine the unknown tension in the thread arising from boundary conditions in the far field (i.e. far away from the pinching neck region); however such a description is not possible in this simple axially-uniform approximation. The recent numerical simulations of Fontelos & Li[51] show that the tensile force in a low-viscosity viscoelastic filament evolving into a beads-on-a-string morphology is in fact $F(t) \approx 3\sigma R(t)$. The (0+1)-dimensional approximation above is thus quite reasonable, and will only result in modest errors in the prefactor of the final result.

Dimensional analysis shows that viscous stresses in the test fluids utilized in the present study are negligible (*Oh* << 1) are negligible; equation (5) then simplifies to the following expression

$$\tfrac{1}{2}\rho\ \dot{R}(t)^2 \sim \frac{\sigma}{R(t)} - \Delta\tau_p(t) \qquad (6)$$

Equation (6) can be expressed in non-dimensional form by scaling stresses with a characteristic capillary pressure, the radius with R_0 and time with the Rayleigh time scale $t^* = \sqrt{\rho {R_0}^3 / \sigma}$. This results in the following expression

$$h^2 \sim \frac{1}{h} - \frac{\Delta\tau_p}{(\sigma/R_0)} \tag{7}$$

where $\tilde{h}(\tilde{t}) = R(t)/R_0$ is the dimensionless thickness of the filament.

In the case of a Newtonian fluid the extra stress $\Delta\tau_p$ is zero, and breakup results from a balance between the capillary driving force which is resisted by the fluid inertia. The solutions to Equation (7) are then of the form $h(\tilde{t}) \sim (\tilde{t}_p - \tilde{t})^{2/3}$ where $\tilde{t}_p$ is the dimensionless Newtonian pinch time at which the filament breaks into two discrete drops. This form of self-similar solution to the equations of motion for an inviscid fluid (Oh << 1) evolving under the action of surface tension was first discussed by Keller & Miksis[53] and analyzed in greater detail by Ting & Keller[54] and Day *et al.*[49].

Recent finite element numerical simulations of the drop pinch-off problem for low viscosity fluids show that this 2/3-power scaling in the minimum radius of the neck is robust and applies over several orders of magnitude in $\tilde{h}(\tilde{t})$ even when other global effects such as over-turning invalidate the slender body assumption [21]. Although the precise details of the drop shapes formed at breakup require a fully non-linear theory incorporating viscous effects close to breakup[47] or a detailed computational study (see for example [21]), experiments with Newtonian fluids and weakly elastic polymer solutions have shown that the time to breakup can be quite accurately obtained from the growth of the primary disturbance [36, 55]. The front factor obtained from full numerical simulations is approximately 0.7 (cf. Figure 3 in Chen et al. [21]), and this value is also found to agree well with an experimental value of 0.8 obtained from our present experiments, as well as other recent experiments with aqueous polymer

solutions[35, 48]. When elastic stresses are absent, equation (7) is therefore expected to have a solution of the functional form (in dimensional variables)

$$h(t) = \frac{R_{mid}(t)}{R_0} \approx 0.8\left(\frac{\sigma}{\rho {R_0}^3}\right)^{1/3}\left(t_p - t\right)^{2/3} \tag{8}$$

We use this result to convert the approximate expression in equation (7) to an equality and now consider the more complex situation that arises when there are polymer additives in the fluid, which result in an additional elastic stresses.

The linear stability of a viscoelastic fluid thread subject to capillary-driven perturbations has been considered in detail for a range of constitutive models[56-58]. In each case, the initial mode of disturbance is found to be essentially unchanged from the Newtonian analog, since the polymer chains are initially unstretched and contribute little stress at short times. This is also in accord with our experimental observations shown in Figs. 2(a) and (b) which show that the initial necking process remains unchanged upon the addition of polymer. We thus combine equation (6) with an appropriate constitutive model. Here we select the single-mode FENE-P dumbbell for simplicity, and the equations for the *zz*- and *rr*- components of the second moment of the dimensionless configuration tensor $\boldsymbol{A}$ for the dumbbells become

$$\begin{aligned} \dot{A}_{zz} &= \left[2\dot{\varepsilon} - f(tr\mathbf{A})/\lambda_1\right]A_{zz} + 1/\lambda_1 \\ \dot{A}_{rr} &= \left[-\dot{\varepsilon} - f(tr\mathbf{A})/\lambda_1\right]A_{rr} + 1/\lambda_1 \end{aligned} \tag{9}$$

where λ_1 is the relaxation of the fluid, $\dot{\varepsilon}(t) = -2\dot{R}(t)/R$ is the stretching rate and $f(tr\mathbf{A}) = 1/\left[1 - (Azz + 2A_{rr})/3N_K\right]$ is the nonlinear spring connector with N_K the number of Kuhn steps. The polymeric contribution to the total stress is given by

$$\Delta\tau_p = nk_BT\, f(tr\mathbf{A})\left[A_{zz} - A_{rr}\right] \tag{10}$$

The number density of chains ($n=cN_A/M_w$) and number of Kuhn steps (N_K) are functions of molecular parameters such as the concentration, molecular weight and chemical structure of the chain. The number of Kuhn steps is calculated according to[27]: $N_K = \alpha(F^2 / C_{\infty Mod})^{0.5/1-\nu}$, where α is the number of chemical bonds per chain. For polyethylene oxide with a repeat unit of [–CH_2CH_2O–], we have $\alpha = 3M_w / M_0$, with M_0 being the molecular weight of the monomer unit). The parameter F is the geometric factor ($F = sin(tan^{-1}(\sqrt{2}))$) and $C_{\infty Mod}$ is the modified characteristic ratio ($C_{\infty Mod} = C_\infty (F^2 / C_\infty)^{2\nu-1}$), modified to account for the non-theta condition of the system. A calculation of the coil expansion factor for PEO gives $C_{\infty Mod} = 4.01$.

A multi-spring model such as the FENE-PM chain could also be considered; however previous studies with highly viscous fluids ($Oh >> 1$) show that the self-governing nature of the elasto-capillary necking process results in a relatively low stretching rate corresponding to $\dot{\varepsilon} \sim 2/(3\lambda_1)$ and the stresses associated with all higher modes relax away[24].

Equations (6) plus (9) and (10) thus make a suitable initial value problem for exploring the crossover between inertio-capillary necking at short times and formation of a cylindrical thread at long times. We recognize of course that such a simplified set of equations cannot capture axial variations along the thread, which would lead to the formation of beads on the cylindrical filament (such as thus observed at very long times in Figure 3(b)). This 'toy' model is thus most suited to experiments with dilute solutions of high molecular solutes which lead to highly elastic fluids ($De >>1$) with low background viscosity ($Oh << 1$). Wagner et al.[48] have also recently presented experiments and numerical simulations for pinching viscoelastic threads using a full 1 dimensional model that establishes the conditions

under which a bead does, or does not, form by comparing the growth rate of the most unstable Rayleigh mode on the cylinder with the necking rate of the filament.

The equation set is integrated using standard methods for stiff sets of differential equations. Typical results for the evolution in the capillary pressure, polymer stress and polymer stretch are shown in Figure 4. Also shown is the dimensionless local rate of stretching which may properly be termed a Weissenberg number $Wi = \lambda_1 \dot{\varepsilon}(t)$ in order to differentiate it from the intrinsic Deborah number, De_0. Initially the polymer molecules are unstretched and the capillary pressure is balanced by inertial acceleration in the fluid column. However close to the Newtonian pinch time t_p determined above, the stretch rate becomes very large in the rapidly necking column and the polymer stretch grows rapidly in the thin filament. At the 'pinch', the elastic stresses grow large enough to resist the diverging capillary pressure. This reduces the rate of necking and the dominant terms in Equation (6) shift to an elasto-capillary balance with negligible inertial effects. This region is identical to that described by Entov & Hinch[24] for viscous polymer solutions (i.e. $Oh >> 1$). The finite extensibility of the molecules is not yet important and the balance between elastic stresses and capillary pressure results in an exponential decrease in the filament radius, with a time constant corresponding to three times the longest relaxation time of the fluid,

$$R = R_p \exp\left[-\frac{(t - t_p)}{3\lambda_1}\right] \tag{11}$$

Here R_p is the radius of the thread at the pinch time t_p and λ_1 is the characteristic time constant of the elasto-capillary necking process.

The exponential decay in time has been observed in viscous polymer solutions corresponding to $Oh >> 1$ [26] and also in low viscosity solutions ($Oh << 1$)[34, 35, 37]. It is worth noting that in

this exponential necking regime, the flow in the thread is a homogeneous uniaxial elongation with a constant extension rate

$$\dot{\varepsilon} = -\frac{2}{R}\frac{dR}{dt} = \frac{2}{3\lambda_1} \tag{12}$$

corresponding to a Weissenberg number $Wi = \lambda_1 \dot{\varepsilon} = 2/3$. This has also been demonstrated by full numerical simulations of the (1+1)-dimensional governing equations for a slender viscoelastic filament[51].

Very close to the final breakup event at t_b the finite extensibility of the molecules becomes important. The nonlinear FENE terms in Equations (9) and (10) have been included in the (0+1) dimensional simulations presented here; however, for the large values of N_K appropriate to the high molecular weight PEO molecules used in the present experiments, the effects of finite extensibility only become significant for $R_{mid}(t)/R_0 \leq 10^{-2}$. The radius will start to decrease linearly in time in this region and rapidly falls below the resolution of the imaging system. Very recent numerical simulations of jet break-up using the Giesekus and FENE-P models and incorporating inertia show the same cross-over at very small length scales from the exponential thinning to an ultimately linear decrease in the radius with time[51].

IV RESULTS

A Comparison with model simulations

In Figure 5(a) we have plotted the evolution of the drop breakup process as it approaches the pinch time, for the Newtonian glycerol-water mixture and solutions of PEO at various molecular weights. All the solutions behave identically in this flow regime and follow the potential flow scaling law of $R_{\min} \propto \tau^{2/3}$, where $\tau = (\tilde{t}_p - \tilde{t})$ is the dimensionless time from

the pinch event, in agreement with previous results.[34, 35, 51, 59] Also shown in the figure is the prediction using the (0+1)-dimension Newtonian pinch model, with the prefactor of 0.8, incorporating the measured values for fluid density of 1080 kg/m^3 and surface tension of 63×10^{-3} N/m [Equation (8)]. It is obvious that the model prediction does indeed show reasonable agreement with the experimental results, albeit with a slight shift of the time scale. The same plot is also shown in Figure 5(b) for the 0.05wt% PEO solution (M_w = 2×10^6 g/mol), with the additional predictions of the inertio-elastic pinch model. Both the Newtonian pinch model and the inertio-elastic model with the Zimm relaxation time show excellent agreement with experimental Newtonian fluid results as the pinch-time is approached, i.e. $(t-t_p)\to 0$.

However, the deviation between the one-dimensional necking model and the experimental measurements at earlier times is not surprising. During the initial stages of droplet separation, the images in Figure 3 show that the filament is not long and slender but in fact of $O(1)$ aspect ratio and must be described by a full 1-dimensional or two-dimensional model (see for example [59]). In addition the initial pendant drop that forms below the nozzle is initially held in place by a quasi-static balance between gravity and surface tension. For a hemispherical drop of radius R_0 to remain attached we require

$$\tfrac{2}{3}\pi R_0^3\rho g \;\le\; 2\pi\sigma R_0 \;,\ \text{or equivalently,}\ \frac{\rho g R_0^2}{3\sigma}\le 1$$

which is true for the present experiments. However as the mass of fluid in the pendant drop is slowly increased by the syringe pump, the quasi-static balance cannot be maintained. The beginning of the pinch-off process is thus driven by gravity, and the fluid that forms the pinch region is also stretched axially by the free-falling motion of the pendant drop to which it is attached. These dynamics are not captured in the (0+1)-dimensional theory discussed above

and require a more detailed computational analysis[59], however the magnitude and duration of the effects can be estimated. The images in Figure 3 show that the volume of the primary drop is much larger than the volume of fluid contained in the thread and thus remains essentially constant in time. If the drop volume corresponds to a sphere with centroid located at an initial axial position $L_0 \approx R_0$ at the onset of the pinching process, then the axial contribution to the stretch rate is, at most, of magnitude $\dot{\varepsilon}_z \approx \dot{L}(t)/L(t) = gt/(R_0 + 0.5gt^2)$, if we ignore any viscous stress in the thread resisting the gravitational acceleration of the drop. The maximum axial (gravitational) stretching rate ($\dot{\varepsilon}_{z,\max} = \sqrt{g/2R_0}$) thus occurs at a time of $t_1 = \sqrt{2R_0/g} \approx 20$ ms for the present geometry. However, the resulting Weissenberg number characterizing the magnitude of the molecular stretching induced by this axial acceleration is $\lambda_z \dot{\varepsilon}_{z,\max} = \lambda_z \sqrt{g/2R_0} << 1$ and consequently the effects of an 'elastic pre-strain' in the molecules and corresponding non-zero contribution to the initial viscoelastic stress in the drop pinch-off problem are negligible. Molecular stretching only becomes important very close to the pinch region. This is further confirmed experimentally by digital image analysis of the location of the centroid (z_c) of the pinching drop with time (not presented here). This analysis shows that the axial displacement of the drop varies according to $z_c = (4.5 \pm 0.5)t^2$ so that there is no retardation in the initial drop acceleration resulting from viscoelasticity. Beyond the point t_1 (corresponding to the point of maximum axial stretching) the (0+1)-dimensional solution presented here should be increasingly accurate[59]: the axial stretching contribution decays and the radial necking rate increases (as seen in Figure 3 when the pinch-off region is approached i.e. $(t - t_p) \to 0$).

The model also correctly predicts the formation of an elastic filament beyond the pinch region due to the elastic stress of the polymer solution resisting further extension. However,

the rate of filament thinning computed in the simulation $\dot{\varepsilon} = -2\dot{R}/R$ is much faster than that found experimentally. This rate is dictated in the computation by the Zimm relaxation time λ_Z of the fluid which is much lower than the effective time constant obtained from the experimental rate of filament radius reduction. Also shown in Figure 5(b) is the model prediction using the *effective relaxation time* λ_{eff} obtained experimentally (see Table 1), instead of the Zimm time. This increase in the relaxation time causes a larger elastic stress in the fluid opposing the capillary pressure and hence an increase in the neck radius as the fluid approaches the pinch region. The predicted radius is much higher than the experimental values, although the rate of radius reduction of the filament formed beyond the pinch is the same as the experimental value, as expected. Therefore it may not be unreasonable to expect that the relaxation time of the fluid as it approaches the pinch has a value somewhere between the Zimm relaxation time and the much larger value (λ_{eff}) found later in the filament thinning process.

We have demonstrated that the simple (0+1)-dimensional theory can capture the salient features of the breakup process including the initial inertial-capillary pinching and the formation of a stabilized elastic thread, we now proceed to compare the evolution of the breakup process for filaments of dilute polymer solutions with different molecular weights and concentrations of PEO.

B Effects of polymer molecular weight

In Figure 6, we show a sequence of images of the filament formed after the pinch region, i.e., $(t - t_p) \geq 0$, for solutions of PEO at various molecular weight and c/c^* ~ 0.5. For PEO

solutions of medium molecular weight between $3\times10^5 \le M_w \le 1\times10^6$ g/mol, a small secondary droplet is always formed between two cylindrical filaments joining the primary drop and the reservoir fluid. This satellite drop exists for most of the filament life-time and observations show similar phenomena for the entire concentration range tested. The rate of reduction in the radius of these two filaments, one joining the primary and secondary droplets and the other joining the secondary drop and reservoir fluid, is found to be very similar and the values reported herein are for the lower filament. The two highest molecular weight solutions of $M_w = 2\times10^6$ and 5×10^6 g/mol (at $c/c^* \sim 0.5$) show no clear secondary drop and a single, axially-uniform cylindrical filament was formed after the pinch region.

The presence or absence of a secondary drop in the filament beyond the pinch region of a viscoelastic fluid exiting a nozzle is dependent on the relative magnitudes of the elastic stress and capillary pressure. Elastic stresses resist the necking process, while capillary pressure strives to reduce the filament radius towards breakup. Such a complex interplay can be seen in the solutions of PEO with $M_w = 2\times10^6$ g/mol. As the concentration of PEO decreases (from $c/c^* \sim 0.5$), there exists a transition concentration (at $c \sim 0.002$wt% or $c/c^* \sim 0.02$) at which the elastic stress is no longer large enough to balance the capillary pressure and a secondary drop forms via surface recoil between the reservoir fluid and the primary drop, in the same manner as observed for the lower molecular weight PEO solutions. However, for the solutions of PEO at $M_w = 2\times10^6$ g/mol and $c > 0.002$wt%, a smooth cylindrical column was observed. This morphological difference is thus both concentration and molecular weight dependent. For high molecular weight and high concentration solutions, the filament does become unstable near the final breakup of the drop, and several small beads connected by yet thinner filaments or threads develop. This ultimate instability and the phenomenon of surface

recoil has been predicted by Chang *et al*.[57] to be iterative in nature and has been discussed in detail in Cooper-White *et al*.[35].

It can be seen from Figure 6 that the filaments exist for longer time and are of increasing length as the molecular weight of the PEO increases, at approximately the same c/c^*. The time evolution of the minimum drop radius up to the pinch region $(t \le t_p)$ and of the filament formed after the pinch is shown in Figure 7(a) for PEO solutions with different molecular weights, at fixed concentration $c/c^* \sim 0.5$. By shifting the time axis of the viscoelastic fluid curves to the Newtonian curve, it is apparent that all the curves coincide with each other and with the Newtonian fluid curve from time $40 \ge (t - t_p) \ge 2$ ms. That is, the initial formation of liquid drop under gravity is identical for all PEO solutions, of differing relaxation times but similar shear viscosity (see Table 1) and surface tension. This similarity exists up to within 2 to 3 ms of the pinch time and is consistent with our theoretical analysis of the inertio-elastic capillary thinning (see Figure 5(b)): at short times, i.e. $t << t_p$, the inertial and capillary stresses balance each other, while the elastic stress is negligible and does not contribute to the evolution of the drop necking process. Hence all fluids behave identically in this flow regime irrespective of their viscoelastic properties, as shown in Figure 5(a).

A careful study of the minimum radius of various PEO solutions in Figure 7(a) shows that just prior to the pinch time, i.e. at $2 \le (t_p - t) \le 3$ ms, there is a slight increase in the dimensionless minimum radius of the PEO solutions compared to the Newtonian fluid, which is particularly noticeable for PEO solutions at $M_w = 2\times10^6$ and 5×10^6 g/mol. This observation is consistent with the simulation results of the inertio-elastic analysis shown in Figure 7(b) for three PEO solutions, using the effective relaxation time λ_{eff} obtained from the experimental

rate of filament radius reduction. The elastic contribution of the polymer only manifests itself at high extension rates as the fluid undergoes rapid necking very close to the pinch region. In this rapidly necking region the macromolecules undergo rapid stretching and the fluid experiences a large increase in elastic stress. This is indicated by the rapid rise in the local Weissenberg number, $Wi = \lambda\dot{\varepsilon}(t)$, as $t \to t_p$ that is shown in Figure 4. The predicted increase in the local Weissenberg number as the inertio-elastic pinch time is approached is an order of magnitude larger than the value at the commencement of the drop formation process, increasing up to a critical value of $Wi_{crit} = \lambda\dot{\varepsilon}_{crit} > 1$ at $t = t_p$. It is this critical extension rate which is instrumental in causing the initial, significant stretching of the polymer molecules, and the resultant large increase in the elastic stress. The supercritical extension rates attained as the pinch time is approached was also noted by Amarouchene *et al*.[34] for their experiments with high molecular weight PEO in water, at what they termed the "transition" point. In this region the dynamics of drop formation changes from a self-similar potential flow with a power-law relationship to an exponential thinning of the filament radius.

After the pinch region, i.e. at time $(t - t_p) > 0$, the filament radius decreases exponentially with time, in agreement with the analysis of the elasto-capillary thinning process. From Figure 7(a) it is apparent that the rate of filament radius reduction is dependent on the molecular weight of the PEO in solutions. The extension rates of the filament forming the neck can be determined in the same manner as utilized in the capillary-thinning and filament-stretching experiments, i.e.

$$\dot{\varepsilon} = -\frac{2}{R}\frac{dR}{dt} = -2\frac{d\,ln(R_{\min}/R_0)}{dt} \tag{13}$$

The filament extension rates observed in the various PEO solutions are given in Table 1; the values are found to decrease with increasing molecular weight of PEO in solutions. From the elasto-capillary thinning theory, the local Weissenberg number of the extending filament is $Wi = \lambda_{\text{eff}}\dot{\varepsilon} = 2/3$, and the effective relaxation time of the PEO chains in the extended state λ_{eff} can thus be determined. The values of λ_{eff} for the PEO solutions (shown also in Table 1) are seen to increase with molecular weight. This is also in qualitative agreement with extensional viscosity measurements obtained from the opposing-jet instrument (see Section 2). It can be seen from Table 1 that the value of λ_{eff} for each solution is also significantly higher than the longest Zimm relaxation time calculated from Equation (3), using the intrinsic viscosity values determined from the Mark-Houwink-Sakurada equation (see Figure 1). This deviation is in accord with the findings of Christanti and Walker[37] for similar PEO solutions undergoing jet breakup under forced disturbances. In Christanti and Walker[37], analysis of the video images showed that the relaxation times determined from the rate of jet radius reduction were a factor of two higher than the Zimm values, although these authors suggested that such differences were more a result of experimental error than a matter of physical significance. It should also be noted here that the Zimm relaxation times quoted by Christanti and Walker[37] were calculated based on a numerical front factor of 0.95 and were higher than they would have been if calculated using the front factor of 0.463 determined for PEO in a good solvent with solvent quality index of 0.55, as used here.

From Equation (3) it is clear that the longest relaxation time is expected to vary with the viscosity of the suspending solvent and the molecular weight of the polymer chains. In Figure 8 we show the values of λ_{eff} obtained for PEO solutions of varying molecular weight scaled with solvent viscosity and plotted as a function of polymer molecular weight. Also shown are the scaling of the longest Zimm relaxation times of these solutions and the data of Christanti

and Walker[37]. The data show the expected scaling with molecular weight, however the values of the relaxation time determined from the rate of filament or jet radial reduction are approximately an order of magnitude higher than expected from Zimm theory. This enhanced relaxation time arises because macromolecules in an extended state will start to interact with one another, even though they are in the dilute concentration regime under equilibrium conditions where no molecular interaction is expected. Moreover, as the polymer molecules are extended and interact with one another, it is to be expected that the extent of the interactions will depend on the concentration in solution, as polymer-polymer interactions will be more prevalent the higher the concentration. Hence it is of interest to examine further the effect of polymer concentration on the effective relaxation time obtained from filament extension during the drop breakup process.

C Effects of polymer concentration

To examine the effect of polymer concentration on the effective relaxation time, we have investigated a series of PEO solutions of $M_w = 1\times10^6$ g/mol of varying concentrations from $0.01 \le c/c^* \le 0.5$ in a solvent of 45wt% glycerol/55wt% water. The solution viscosity and composition of these solutions are given in Table 2. The shear viscosities of the solutions vary between 8.2×10^{-3} and 4.7×10^{-3} Pa.s and the equilibrium surface tension for all the solutions is approximately 57×10^{-3} N/m, while the dynamic surface tension has been found to vary weakly with concentration of PEO in the solutions (see Figure 2). The evolution of the minimum radius during the approach to the pinch time and during the formation of subsequent filament is shown in Figure 9 as a function of the shifted time. It is clear that for these solutions with varying PEO concentration, the initial evolution of the drop radius as it approaches the inertio-elastic pinch is similar to the Newtonian fluid until within 1 to 2 ms of

the pinch time, as found for the solutions with varying PEO molecular weight. After the pinch region all PEO solutions show an enhanced resistance to pinch-off and form a thin filament which exists for various lengths of time, from 1 to 2 ms for the lowest concentration of 0.002wt% PEO ($c/c^* = 0.012$) to over 40 ms for the highest concentration of 0.1 wt% ($c/c^* = 0.62$).

A close inspection of Figure 9 indicates that there is an anomalous behaviour with the solutions of 0.01wt% PEO and lower; the radius of the rapidly shrinking neck appears to reduce faster than the analogous Newtonian fluid very close to the pinch region, i.e., $1 \le (t_p - t) \le 2$ ms. This is in contrast to the wider neck arising from the presence of the elastic stress that was observed for the series of PEO solutions with varying molecular weight and also for the solutions of 1×10^6 g/mol PEO at higher concentrations. This more rapid reduction in the neck radius on approach to the pinch region could be due either to the slightly lower shear viscosity of these solutions (due to the lower polymer concentrations in the same solvent), or to the somewhat higher dynamic surface tension at short times on the order of tens of milliseconds.

It is also apparent from Figure 9 that after the inertia-elastic pinch, the rate of filament radius reduction is a function of polymer concentration. The measured extension rates of the filament and the effective relaxation times obtained from these extension rates are given in Table 2. These relaxation times are found to be a strong function of polymer concentration even in the dilute region. This variation in the effective relaxation time has also been noted in other studies of low viscosity polymer solutions undergoing similar drop breakup[34], as well as in the capillary thinning device[29, 30]. However, as shown in Figure 2, there is a significant difference in the surface tension of the PEO solutions of differing concentrations up to

$\Delta\sigma = \pm 10^{-2}$ N/m at intermediate surface age of between 10^2 and 10^4 ms. In order to ascertain that the variation in the rates of filament thinning found for the different PEO solutions are not due to this difference in dynamic surface tension, we have also carried out drop formation experiments using PEO solutions in the same glycerol-water mixture, but with 0.4wt% 2-butanol added. The addition of 2-butanol has the effect of decreasing the DST at short times of the solutions to the same value as the equilibrium value (see Figure 2), while maintaining the shear viscosity of the solutions. For example, the surface tension for the 0.02wt% PEO is reduced from 68×10^{-3} N/m to 60×10^{-3} N/m at the minimum measurable surface age of 10 ms.

These solutions with the added 2-butanol show almost identical filament formation characteristics with the PEO solutions without the added 2-butanol (see Figure 9). Therefore it may be deduced that differences in the dynamic surface tension of the PEO solutions are not the cause of the observed differences in the evolution of the filament after the inertio-elastic pinch. Although slight differences in the actual rates determined from the filament thinning process were noted between the solutions with and without 2-butanol (see Table 2), these differences are well within the experimental errors in the determination of the rate of filament thinning.

Before proceeding further with the discussion of the effective relaxation times, it is worth considering the errors involved in the determination of these relaxation times. It can be assumed that most of the errors involved in the determination of the relaxation times arise from the determination of the filament thinning rate. These errors can be estimated as follows: Using the maximum magnification available with the present image capturing technique the root mean square error in determining the filament radius (or diameter) can be estimated to be initially ±5 to ±10% (that is, ±2 pixels from an image spanning 20 to 40

pixels depending on the solution) at the start of the filament thinning process immediately after the pinch, and ±20% (or ±2 out of 10 pixels) just prior to break-off or at the point below which further measurements are deemed too inaccurate, i.e. when $R_{min}/R_0 = O(0.02)$. The rate of necking is the slope of the semi-log plot of the radius against time and the maximum error in the rate is then the square root of the sum of square of the two errors involved in determining the radius, giving a total of ±23% error. The actual variation obtained from several repeated measurements of the rate of radius reduction, using either the same solution or two separately prepared solutions, showed a similar error of approximately ±20% in several cases. Hence this value is used as an estimate of the errors in the determination of the effective relaxation times. Smaller errors could be obtained if the magnification during the image capturing of the drop breakup process is increased from that used in the present experiments, at the detriment of losing visual information on the overall pinch-off process.

We can now proceed to investigate the effects of polymer concentration on the effective relaxation time obtained from the rate of necking. The effective relaxation times scaled with solvent viscosity for solutions of PEO with molecular weight of $M_w = 1\times10^6$, 2×10^6 and 5×10^6 g/mol are shown in Figure 10. All of the solutions show an increase in the effective relaxation time with polymer concentration, showing a power law relationship with an exponent of approximately 0.65 regardless of the molecular weight tested. This is lower than the power law exponent (~ 0.8) found by Amarouchene *et al.*[34] and Bazilevskii *et al.*[30] on other solutions of PEO. Stelter *et al.*[29] also reported the relaxation times of PEO solutions determined from radius reduction in a self-thinning capillary breakup experiment to be dependent on the PEO concentration, although no value of the exponent was given.

The results for the PEO solutions shown in Figure 10 and Table 2 indicate that the effective relaxation times obtained from filament thinning are up to 10 times the longest Zimm relaxation time at the highest PEO concentration investigated, i.e., at $c/c^* \sim 0.5$. A plot of the effective relaxation time, scaled with the longest Zimm relaxation time (λ_{eff}/λ_Z), as a function of polymer concentration relative to the overlap concentration (c/c^*) is shown in Figure 11 for all of the PEO solutions studied. Also shown are the error bars of $\pm 20\%$ for the data of PEO at $M_w = 1\times10^6$, 2×10^6 and 5×10^6 g/mol. It should also be noted that the standard errors in the determination of the effective relaxation time for the very dilute solutions are probably somewhat larger than those shown, due to the extremely fast rate of filament shrinkage which occurred within a time scale of the order of 2 to 3 ms. But despite the relatively large errors involved, the increase in the ratio λ_{eff}/λ_Z is statically significant and the ratio increases from the expected value of unity for $c/c^* < 0.01$ to values above 10 as polymer concentration increases.

V DISCUSSION

We have now seen that polymer chain interactions in the stretched state can affect the solution relaxation time, which is manifested as an increase in the effective relaxation times over the theoretical Zimm values determined from the equilibrium, coiled-state. It is then of further interest to ask if these chain-chain interaction effects are dependent on the absolute concentration or if there is a universal dependence of the interactions on the reduced concentration c/c^* as mooted by Harrison *et al.*[60] The results for PEO solutions shown in Figure 10 and Tables 1 and 2 indicate that the effective relaxation times obtained from the rate of filament thinning are up to 10 times the longest Zimm relaxation time at the highest PEO concentration of c/c* ~ 0.5. In Figure 11 the effective relaxation times scaled with the

Zimm times ($\lambda_{\text{eff}} / \lambda_Z$) are plotted as a function of the reduced concentration (c/c^*). The results of all the solutions studied in this work all fall on this master curve with the exception of the solution of 3×10^5 g/mol PEO (Note that the data for the 3×10^5 g/mol PEO have been obtained with two separately prepared solutions at the same concentration, with the two giving the same filament stretching rate and effective relaxation time. Hence the noted deviation is most likely due to the large errors involved in the determination of the effective relaxation time of this low molecular weight PEO with very short life time of the filament of the order of 5 to 6 ms). By plotting the ratio of the effective relaxation time to the Zimm time, we have effectively scaled the measured relaxation times with both the solvent viscosity and polymer molecular weight and, as a result, the data for PEO of all molecular weights fall on the same master curve, with $\lambda_{\text{eff}} / \lambda_Z$ approaching unity as $c/c^* \to 0.01$. Thus, the dimensionless effective relaxation time appears to be a universal function of the extent of polymer-polymer interactions regardless of the absolute concentration, as expected, at least for this polymer. It would be interesting to check if this universality applies to other polymers, either linear or branched, or with varying solvent effect. A linear regression of all the data up to $c/c^* = 0.5$ (with the exception of the results for the PEO solutions at M_w = 3×10^5 g/mol) gives a line of best fit with a power-law exponent of 0.65. We have also included the results of Amarouchene *et al.*[34] and Christanti and Walker[37] for low viscosity PEO solutions in the figure (using values of λ_Z and c^* estimated in the same manner as for our solutions). Note that these results overlay our line of best fit over the range of c/c^* investigated, although Amarouchene *et al.*[34] have suggested that the power-law exponent is closer to 0.8.

Under quiescent conditions, all of the PEO solutions studied in the present work are in the dilute regime with $c/c^* < 1$. However, when undergoing extension in the necked filament,

the solutions appear to exhibit semi-dilute solution behaviour arising from chain-chain interactions with a concentration-dependent relaxation time scale. As the macromolecules in solutions are unravelled from the equilibrium coiled configuration on approach to the pinch region (and also subsequently during filament stretching), they will increasingly feel the presence of the surrounding molecules. These interactions will be enhanced as the concentration increases. In the stretched state, the transition from dilute to semi-dilute concentration regimes will occur at a much lower value than indicated by the value of c^* determined in the quiescent state, by using the intrinsic viscosity values of Figure 1, for example. It is only in the so-called "ultradilute" region[60] where absence of chain-chain interaction of polymer in the stretched state may truly exist. Harrison *et al*.[60] found, using birefringence measurements for flow through a two-roll mill, that chain-chain interactions inhibit polystyrene molecules from attaining full extension in their solution at $c/c^* \sim 0.1$, in contrast to that found for a true ultradilute concentration of $c/c^* \sim 0.01$. The results obtained in the present study indicate that the solutions are approaching the true dilute region even in the stretched state as $c/c^* \sim 0.01$, in agreement with the measurements of Harrison *et al*.[60] However, due to limits in temporal and spatial resolution it may not be possible to use these drop breakup experiments to determine the concentration limit below which no polymer concentration effects exist even in the stretched state. None of the earlier studies[29, 30, 34] were able to arrive at concentrations of PEO low enough to yield a concentration-independent relaxation time. This may be attributed to a lack of spatial and temporal resolution for the solutions at very low polymer concentration, or to an insufficiently large polymeric contribution to the total fluid stress which prevents a clear crossover from an inertio-capillary to elasto-capillary balance.

Also shown in Figure 11 is the simplest possible correction to the Zimm result (Equation (3)) obtained by replacing the solvent viscosity by the zero-shear-rate viscosity $\eta_0 = \eta_s \{1 + c[\eta].....\}$. It is obvious that the factor $(1 + c/c^*)$ suggested from such a mean field approximation is not sufficient to capture the significant variation observed experimentally. Another possible correction is to recognize that the longest time constant will vary with the drag on the elongated polymer coils as they deform. We can estimate this change in the drag by using the ratio of the drag on a straight rod to that on a Gaussian coil; i.e. $\frac{\zeta_{\max}}{\zeta_0} = \frac{\zeta_{rod}}{\zeta_{coil}} = \frac{6.28L}{5.11R\ln(L/d)}$ [27], where L is the length of the fully extended chain, d is the diameter (~ 4.9 Å) and R is the equilibrium root-mean-square end-to-end separation of the chain. This ratio $\zeta_{\max}/\zeta_0$ depends on the molecular weight as it affects the values of both L ($= N_k a$) and R ($= N_k^{\nu} a$) used in the calculation, but the variation is not significant for the range of molecular weights from 1×10^6 to 5×10^6 g/mol. From Figure 11 the rod/coil drag scaling $\left(1 + \frac{\zeta_{rod}}{\zeta_{coil}}\frac{c}{c^*}\right)$ for a typical PEO of $M_w = 2\times10^6$ g/mol is shown and it is obvious that the effect of changing the drag on a single polymer chain from coil to rod configuration alone is also insufficient to account for the chain-chain interaction effects. At present it is still unclear how to develop a molecular theory that accounts for the chain-chain intermolecular interactions. However one can argue that the principal change is an increase in the number of frictional events acting on a partially unravelled chain due to neighbouring chains. The polymer contribution to the viscosity should thus scale no longer with the number density of chains per unit volume ($\nu = cN_A k_B T / M_w$), but with the number of (possibly overlapping) chain segments (cM_w) per unit volume. The data available in the present study and other recent studies is certainly consistent with an effective relaxation time that scales as

$(\lambda / \lambda_Z) \sim (c/c^*)^{3\nu-1}$. However, further theoretical work is required to ascertain the appropriate scaling law for interchain dilute solutions undergoing extensional flows.

VI CONCLUSIONS

We have investigated the drop formation dynamics of a series of low viscosity elastic fluids, which were controlled to have very similar shear viscosity and surface tensions but differ substantially in viscoelastic properties. For these low viscosity fluids, viscous and elastic stresses are irrelevant prior to the rapid formation of the pinch region, during which the dynamics are controlled by an inertial-capillary balance. The rapid decrease in the radius on approach to break-off produces large increases in the extension rate at this location. We have demonstrated that even at very dilute concentrations, the polymer molecules can be highly extended during the approach to the pinch region without viscous effects being important. As a result of this significant molecular extension, the elastic stress grows to match the capillary pressure, preventing the neck from breaking off, in contrast to the corresponding Newtonian fluid. This stabilization of the pinch region results in two cylindrical filaments which develop either side of a secondary drop between the nozzle and the primary drop. Alternatively the pinch region may form a single cylindrical filament without any secondary drop, depending on polymer molecular weight and concentration. Regardless of the specific morphology, an elastic-capillary balance holds in these cylindrical filaments and the radius decreases exponentially with time. A simple zero-dimensional model captures this transition and shows that the local Weissenberg number is $Wi = \lambda \dot{\varepsilon}(t) \simeq 2/3$ subsequent to the pinching event is valid during the filament stretching event. The effective relaxation times obtained from this expression are up to an order of magnitude higher than the estimated Zimm relaxation times for all PEO solutions studied and only approach the Zimm relaxation time when $c/c^* \leq 0.01$.

In this exponential stretching regime, inter-molecular interactions result in relaxation times far above equilibrium predictions. A universal scaling with reduced concentration c/c^* is observed over a wide range of concentrations and molecular weights. This effective relaxation time in extension is shown in Figure 11 and can be described by a relationship of the form

$$\frac{\lambda_{\text{eff}}}{\lambda_Z} = 0.463 \frac{[\eta] M_{\text{w}} \eta_s}{N_A k_B T} \left(\frac{100c}{c^*} \right)^{0.65} \quad \text{for } 0.01 \le c/c^* \le 1 \tag{14}$$

where $[\eta]$ and c^* both vary with molecular weight according to Equations (1) and (2), respectively.

References

[1]Guthrie, C., "On drops". Proc. R. Soc. London. 13, 444 (1864).

[2]Rayleigh, L., "Investigations in capillarity". Phil. Mag. 48, 321 (1899).

[3]Tate, T., "On the magnitude of a drop of liquid formed under different circumstances". Philos. Mag. 27, 176 (1864).

[4]Bruce, C.A., "Dependence of ink-jet dynamics on fluid characteristics". IBM J. Res. Dev. 20, 258 (1976).

[5]Young, B.W., "Pesticide Formulations and Application Systems". ASTM STP. 5, 13 (1986).

[6]Peregrine, D.H., G. Shoker, and A. Simon, "The bifurcation of liquid bridges". J. Fluid Mech. 212, 25 (1990).

[7]Shi, X.D., M.P. Brenner, and S.R. Nagel, "A cascade of structure in a drop falling from a faucet". Science. 265, 219 (1994).

[8]Zhang, X. and O.A. Basaran, "An experimental study of dynamics of drop formation". Phys. Fluids. 7, 1184 (1995).

[9]Wilkes, E.D., S.D. Phillips, and O.A. Basaran, "Computational and experimental analysis of dynamics of drop formation". Phys. Fluids. 11, 3577 (1999).

[10]Rao, E.V.L.N., R. Kumar, and N.R. Kuloor, "Drop formation in liquid-liquid systems". Chem. Eng. Sci. 21, 867 (1966).

[11]Edgerton, H.E., E.A. Hauser, and W.B. Tucker, "Studies in drop formation as revealed by the high-speed camera". J. Phys. Chem. 41, 1017 (1937).

[12]Wilkes, E.D. and O.A. Basaran, "Forced oscillations of pendant (sessile) drops". Phys. Fluids. 9, 1512 (1997).

[13]Brenner, M.P., J. Eggers, K. Joseph, S.R. Nagel, and X.D. Shi, "Break-down of scaling in droplet fission at high Reynolds numbers". Phys. Fluids. 9, 1573 (1997).

[14]Badie, R. and D.F.d. Lange, "Mechanism of drop constriction in an drop-on-demand inkjet system". Proc. R. Soc. Lond. A. 453, 2573 (1997).

[15]Bechtel, S.E., M.G. Forest, and K.J. Lin, "Closure to all orders to 1-D models for slender viscoelastic jets: An integral theory for axisymmetric, torsionless flow". Stability Appl. Anal. Cont. Media. 2, 59 (1992).

[16]Eggers, J. and T.F. Dupont, "Drop formation in a one-dimensional approximation of the Navier-Stokes equation,". J. Fluid Mech. 262, 205 (1994).

[17]Papageorgiou, D.T., "On the breakup of viscous liquid threads". Phys. Fluids. 7, 1529 (1995).

[18]Schulkes, R.M.S.M., "The evolution and bifurcation of a pendant drop". J. Fluid Mech. 278, 83 (1994).

[19]Zhang, D.F. and H.A. Stone, "Drop formation in viscous flows at a vertical capillary tube". Phys. Fluids. 9, 2234 (1997).

[20]Gueyffier, D., J. Li, A. Nadim, R. Scardovelli, and S. Zaleski., "Volume-of-fluid interface tracking with smoothed surface stress methods for three-dimensional flows". Comput. Phys. 152, 423 (1999).

[21]Chen, A.U., P.K. Notz, and O.A. Basaran, "Computational and experimental analysis of pinch-off and scaling". Phys. Rev. Lett. 88(17), 174501 (2002).

[22]Bazilevskii, A.V., V.M. Entov, and A.N. Rozhkov. *Liquid filament microrheometer and some of its applications.* in *Third European Rheology Conference*. 1990: Elsevier Applied Science.

[23]Liang, R.F. and M.R. Mackley, "Rheological characterization of the time and strain dependence for polyisobuthylene solutions". J. Non-Newt. Fluid Mech. 52, 387 (1994).

[24]Entov, V.M. and E.J. Hinch, "Effect of a spectrum of relaxation times on the capillary thinning of a filament of elastic liquids"". J. Non-Newt. Fluid Mech. 72, 31 (1997).

[25]McKinley, G.H. and A. Tripathi, "How to extract the Newtonian viscosity from capillary breakup experiments in a filament rheometer". J. Rheol. 44(3), 653 (2000).

[26]Anna, S.L. and G.H. McKinley, "Elasto-capillary thinning and breakup of model elastic liquids". J. Rheol. 45, 115 (2001).

[27]Larson, R.G., "The Structure and Rheology of Complex Fluids". Oxford University Press, Oxford (1999).

[28]Stelter, M., T. Wunderlich, S.K. Rath, G. Brenn, A.L. Yarin, R.P. Singh, and F. Durst, "Shear and extensional investigation in solutions of grafted/ungrafted amylopectin and polyacrylamide". J. Polym. Sci. 74, 2773 (1999).

[29]Stelter, M., G. Brenn, A.L. Yarin, R.P. Singh, and F. Durst, "Investigation of the elongation behaviour of polymer solutions by means of an elongational rheometer". J. Rheol. 46(2), 507 (2002).

[30]Bazilevskii, A.V., V.M. Entov, and A.N. Rozhkov, "Breakup of an Oldroyd liquid bridge as a method for testing the rheological properties of polymer solutions". Polym. Sci. Ser. A. 43(7), 716 (2001).

[31]Schümmer, P. and K.H. Tebel, "The new elongational rheometer for polymer solutions". J. of Non-Newt. Fluid Mech. 12, 331 (1983).

[32]Li, J. and M.A. Fontelos, "Drop dynamics on the beads-on-string structure for viscoelastic jets: A numerical study". Phys. Fluids. 15, 922 (2003).

[33]Clasen, C., J. Eggers, M.A. Fontelos, J.Li, and G.H. McKinley, "The beads-on-string structure of viscoelastic threads". J. Fluid Mech. In Press (2005).

[34]Amarouchene, Y., D. Bonn, J. Meunier, and H. Kellay, "Inhibition of the finite-time singularity during drop fission of a polymeric fluid". Phys. Rev. Lett. 86(16), 3558 (2001).

[35]Cooper-White, J.J., J.E. Fagan, V. Tirtaatmadja, D.R. Lester, and D.V. Boger, "Drop formation dynamics of constant low-viscosity, elastic fluids". J. Non-Newt. Fluid Mech. 106(1), 29 (2002).

[36]Mun, P.R., J.A. Byars, and D.V. Boger, "The effect of polymer concentration and molecular weight on the breakup of laminar capillary jets". J. Non-Newt. Fluid Mech. 74, 285 (1998).

[37]Christanti, Y. and L.M. Walker, "Effect of fluid relaxation time of dilute polymer solutions on jet break-up due to a forced disturbance". J. Rheol. 46(3), 733 (2002).

[38]Stokes, J.R., Swirling Flow of Viscoelastic Fluids. 1998, University of Melbourne.

[39]Crooks, R.C., J.J. Cooper-White, and D.V. Boger, "The role of dynamic surface tension and elasticity on the dynamics of drop impact". Chem. Eng. Sci. 56, 5575 (2001).

[40]Ferguson, J., N.E. Hudson, and B.C.H. Warren, "The break-up of fluids in an extensional flow field". J. of Non-Newt. Fluid Mech. 44, 37 (1992).

[41]Brandrup, J., E.H. Immergut, and W. McDowell, eds. *Polymer Handbook*. 1975, Wiley: New York.

[42]Doi, M. and S.F. Edwards, "The Theory of Polymer Dynamics". Oxford University Press, New York (1986).

[43]Graessley, W.W., "Entangled linear, branched and network polymer systems - molecular theories". Adv. Polym. Sci. 47, 67 (1982).

[44]Öttinger, H.C., "Stochastic Processes in Polymeric Liquids". Springer-Verlag, Berlin (1996).

[45]Cooper-White, J.J., R.C. Crooks, K. Chockalingam, and D.V. Boger, "Dynamics of polymer-surfactant complexes: elongational properties and drop impact behaviour". Ind. Eng. Chem. Res. 41(25), 6443 (2002).

[46]Funada, T. and D.D. Joseph, "Viscoelastic potential flow analysis of capillary instability". J.Non-Newt. Fluid Mech. 111(2-3), 87 (2003).

[47]Eggers, J., "Nonlinear dynamics and breakup of free-surface flows". Rev. Mod. Phys. 69, 865 (1997).

[48]Wagner, C., Amarouchene, Y., Bonn, D. and Eggers, J., "Droplet Detachment and Satellite-Bead Formation in Viscoelastic Fluids". Phys. Rev. Lett. (Submitted), (2005).

[49]Day, R.F., E.J. Hinch, and J.R. Lister, "Self-similar capillary pinchoff of an inviscid fluid". Phys. Rev. Lett. 80, 704 (1998).

[50]Notz, P.K., Basaran, O.A., "Dynamics and breakup of a contracting liquid filament". Journal Fluid Mech. 512, 223 (2004).

[51]Fontelos, M.A. and J. Li, "On the evolution and rupture of filament in Giesekus and FENE models". Journal Non-Newt. Fluid Mech. 118, 1 (2004).

[52]Renardy M, R.Y., "Similarity solutions for breakup of jets of power law fluids". J. of Non-Newt. Fluid Mech. 122(1-3), 303 (2004).

[53]Keller, J.B. and M.J. Miksis, "Surface tension driven flows". SIAM J. Appl. Math. 43, 268 (1983).

[54]Ting, L. and J.B. Keller, "Slender Jets and Thin Sheets with Surface Tension". SIAM J. Appl. Math. 50((6)), 1533 (1990).

[55]Taub, H.H., "Investigation of nonlinear waves on liquid jets". Phys. Fluids. 19, 1124 (1976).

[56]Middleman, S., "Stability of a viscoelastic jet". Chem. Eng. Sci. 20, 1037 (1965).

[57]Chang, H.-C., E.A. Demekhin, and E. Kalaidin, "Iterated stretching of viscoelastic jets". Phys. Fluids. 11(7), 1717 (1999).

[58]Bousfield, D.W., R. Keunings, G. Marucci, and M.M. Denn, "Nonlinear analysis of the surface tension driven breakup of viscoelatic filaments". J. Non-Newt. Fluid Mech. 21(1), 79 (1986).

[59]Ambravaneswaran, B., E.D. Wilkes, and O.A. Basaran, "Drop formation from a capillary tube: Comparison of one-dimensional and two-dimensional analyses and occurrence of satellite drops". Phys. Fluids. 14(8), 2606 (2002).

[60]Harrison, G.M., J. Remmelgas, and L.G. Leal, "Comparison of dumbbell-based theory and experiment for a dilute polymer solution in a corotating two-roll mill". J. Rheol. 43(1), 197 (1998).

M_w (g/mol)	c (wt%)	$[\eta]$ (ml/g)	c/c^*	η_s (Pa.s)	η (Pa.s)	λ_Z (s)	λ_{eff} (s)	λ_{eff}/λ_Z	Oh	De_0
3×10^5	0.20	2.61×10^2	0.56	0.0034	0.0057	5.1×10^{-5}	1.4×10^{-3}	26.89	1.56×10^{-2}	4.29×10^{-3}
6×10^5	0.17	4.10×10^2	0.75	0.0034	0.0059	1.6×10^{-4}	1.9×10^{-3}	11.64	1.61×10^{-2}	1.35×10^{-2}
1×10^6	0.10	5.72×10^2	0.62	0.0034	0.0058	3.7×10^{-4}	4.7×10^{-3}	12.79	1.58×10^{-2}	3.13×10^{-2}
2×10^6	0.05	8.97×10^2	0.48	0.0034	0.0050	1.2×10^{-3}	1.4×10^{-2}	12.13	1.37×10^{-2}	9.83×10^{-2}
5×10^6	0.03	1.63×10^3	0.53	0.0034	0.0051	5.3×10^{-3}	3.5×10^{-2}	6.74	1.39×10^{-2}	4.46×10^{-1}

Table 1 Composition and other properties of polyethylene oxide (PEO) solutions at various molecular weights.

M_w (g/mol)	c (wt%)	$[\eta]$ (ml/g)	c/c^*	η_s (Pa.s)	η (Pa.s)	λ_Z (s)	λ_{eff} (s)	λ_{eff}/λ_Z	Oh	De_0
1×10^6	0.10	5.72×10^2	0.63	0.0047	0.0082	5.1×10^{-4}	7.1×10^{-3}	13.88	2.26×10^{-2}	4.22×10^{-2}
1×10^6	0.05	5.72×10^2	0.31	0.0047	0.0063	5.1×10^{-4}	4.3×10^{-3}	8.37	1.73×10^{-2}	4.22×10^{-2}
1×10^6	0.02	5.72×10^2	0.13	0.0047	0.0055	5.1×10^{-4}	3.1×10^{-3}	6.16	1.51×10^{-2}	4.22×10^{-2}
1×10^6	0.01	5.72×10^2	0.06	0.0047	0.0050	5.1×10^{-4}	1.6×10^{-3}	3.06	1.38×10^{-2}	4.22×10^{-2}
1×10^6	0.005	5.72×10^2	0.03	0.0047	0.0048	5.1×10^{-4}	8.6×10^{-4}	1.68	1.32×10^{-2}	4.22×10^{-2}
1×10^6	0.002	5.72×10^2	0.01	0.0047	0.0047	5.1×10^{-4}	5.5×10^{-4}	1.08	1.29×10^{-2}	4.22×10^{-2}

Table 2 Composition and other properties of polyethylene oxide (PEO) solutions of $M_w = 1\times10^6$ g/mol at various concentrations.

List of Figures

10. Scaled effective relaxation time ($\lambda_{\text{eff}} / \eta_s$) against concentration (c) for PEO solutions of $M_w = 1\times10^6$, 2×10^6 and 5×10^6 g/mol (Lines are drawn as guide only).

11. Scaled effective relaxation time ($\lambda_{\text{eff}} / \lambda_Z$) against dimensionless concentration (c/c^*) for all PEO solutions, showing line of best fit and lines for scaling with $\left(1+\frac{c}{c^*}\right)$ and $\left(1+\frac{\zeta_{rod}}{\zeta_{coil}}\frac{c}{c^*}\right)$.

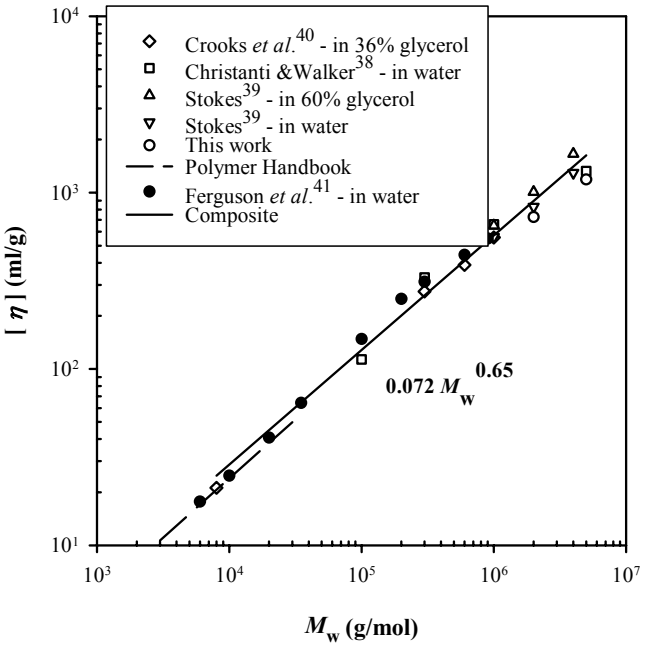

Figure 1 - Tirtaatmadja (Physics of Fluids)

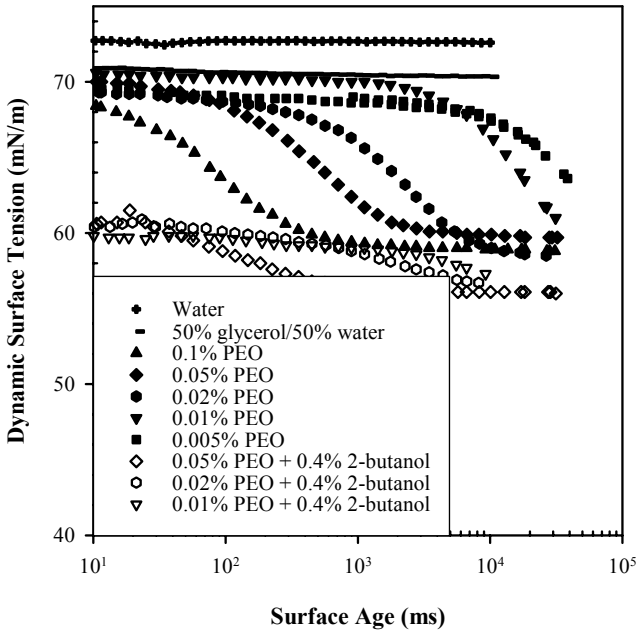

Figure 2 - Tirtaatmadja (Physics of Fluids)

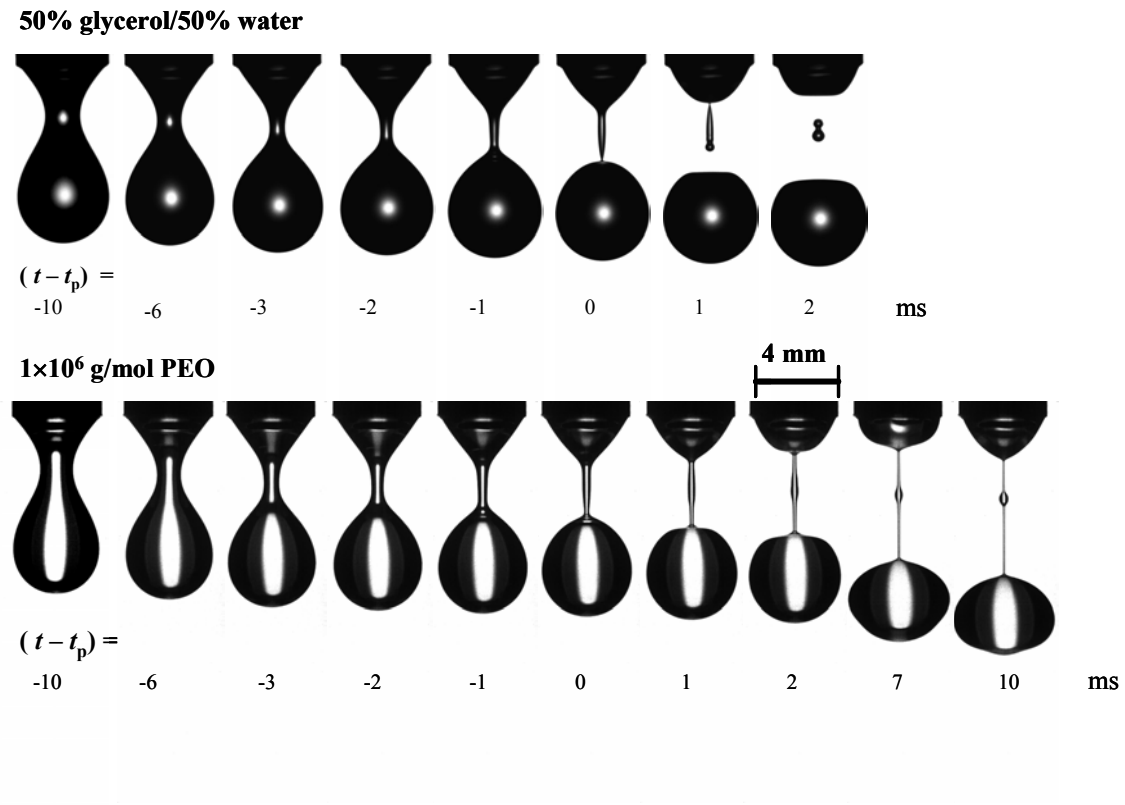

Figure 3 - Tirtaatmadja (Physics of Fluids)

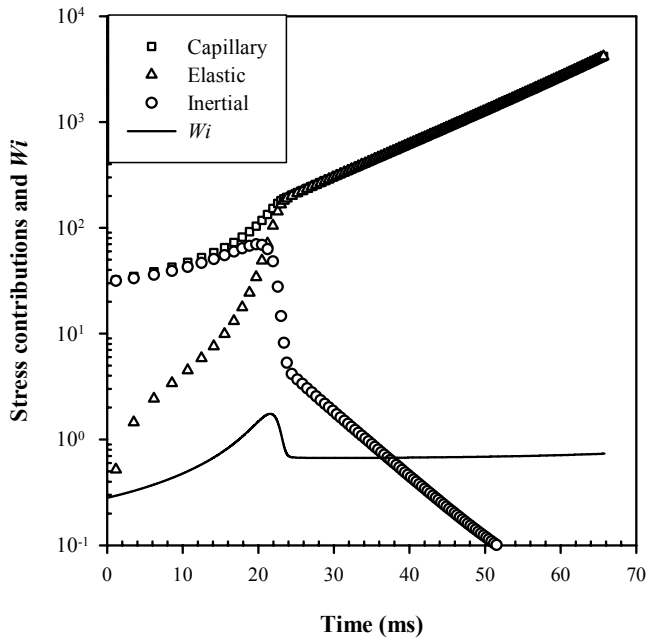

Figure 4 - Tirtaatmadja (Physics of Fluids)

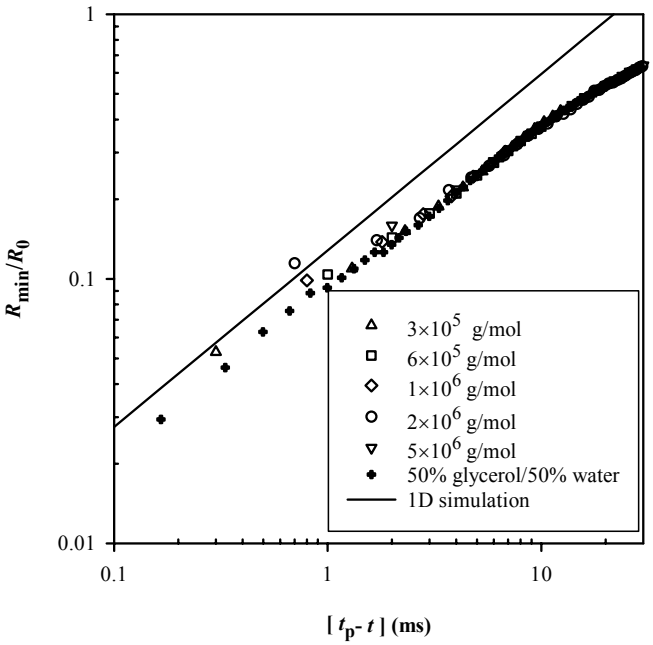

Figure 5(a) - Tirtaatmadja (Physics of Fluids)

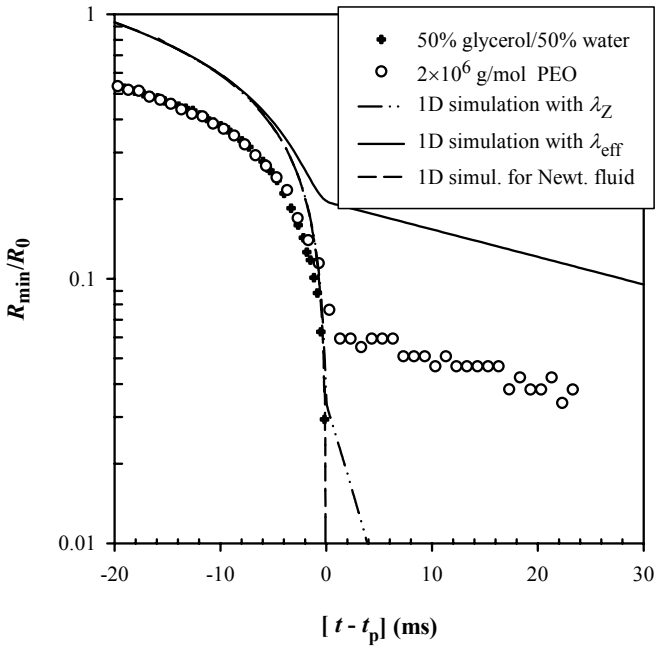

Figure 5(b) - Tirtaatmadja (Physics of Fluids)

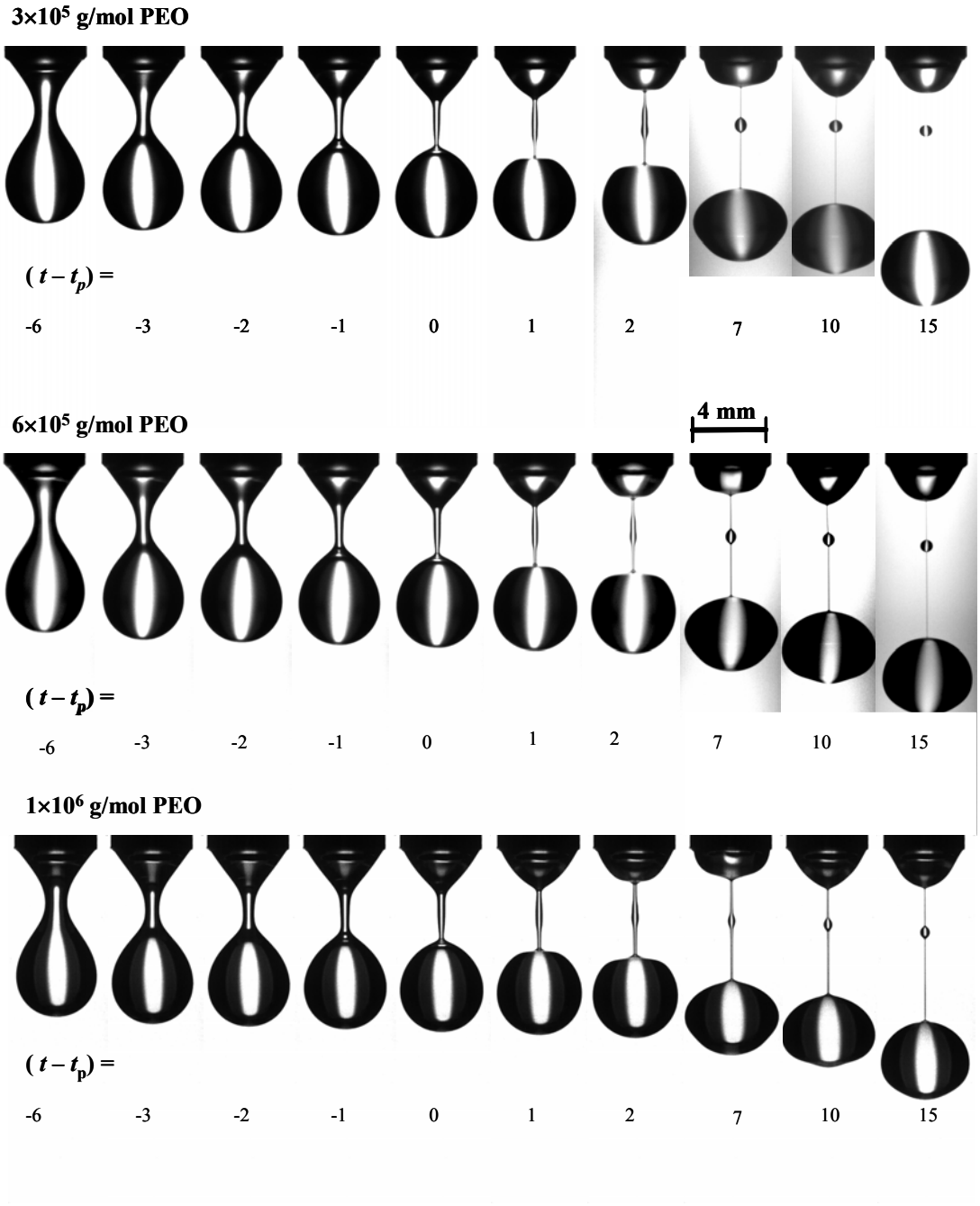

Figure 6 – Tirtaatmadja (Physics of Fluids)

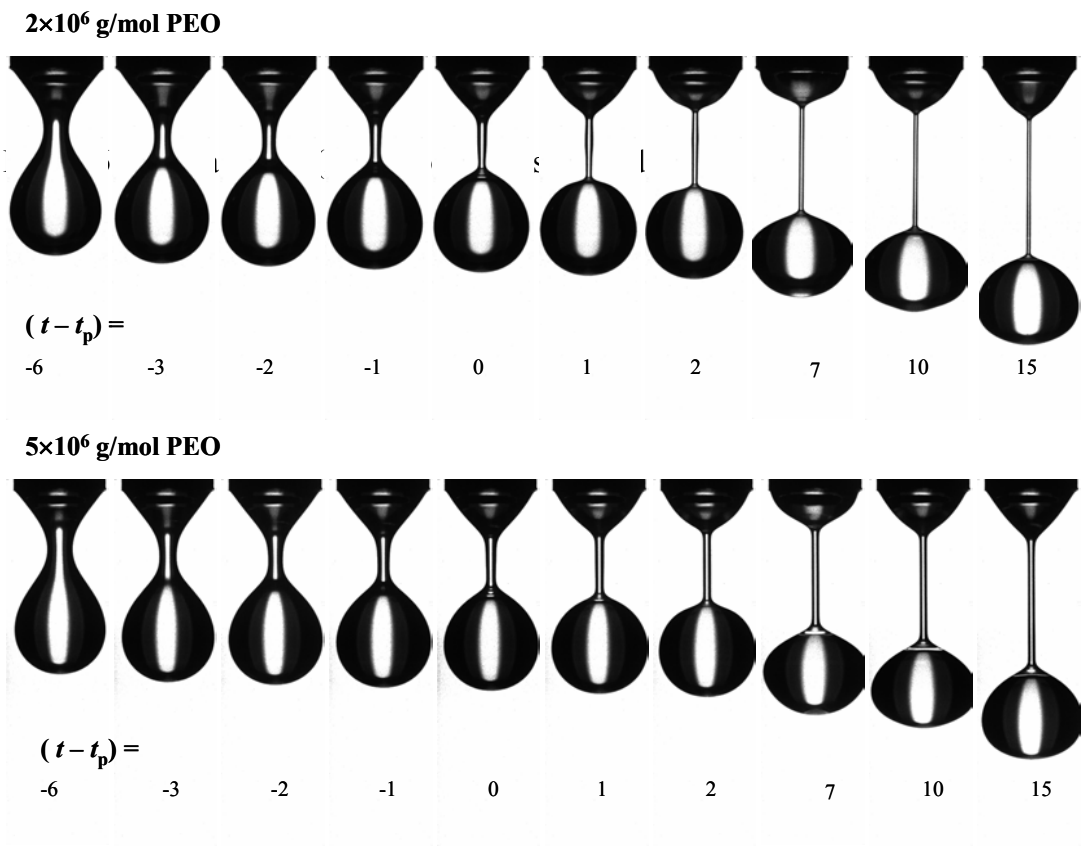

Figure 6 – Tirtaatmadja (Physics of Fluids) – cont'd

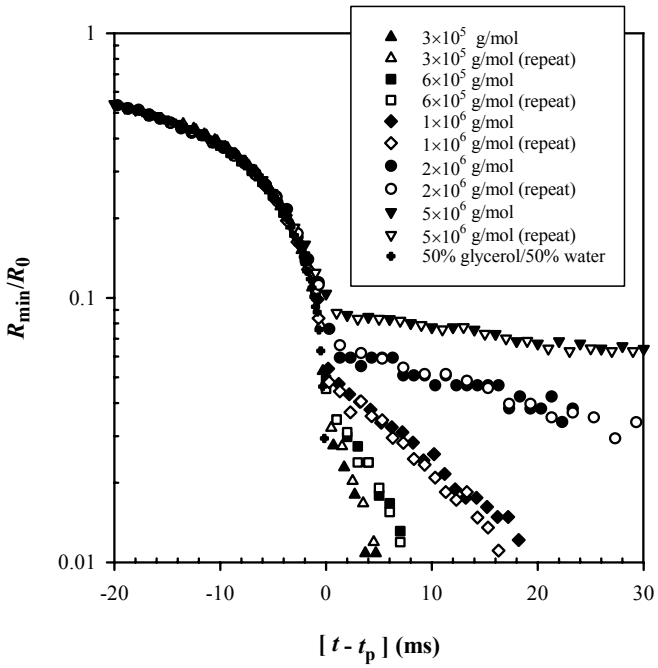

Figure 7(a) - Tirtaatmadja (Physics of Fluids)

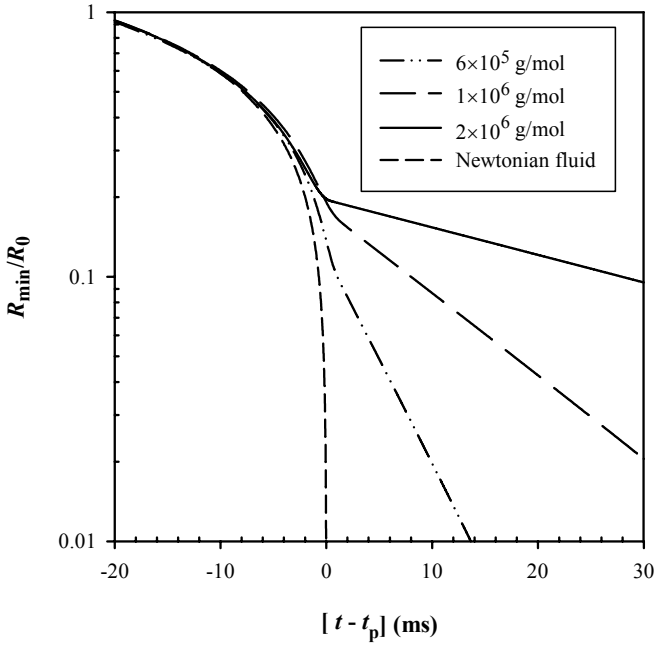

Figure 7(b) - Tirtaatmadja (Physics of Fluids)

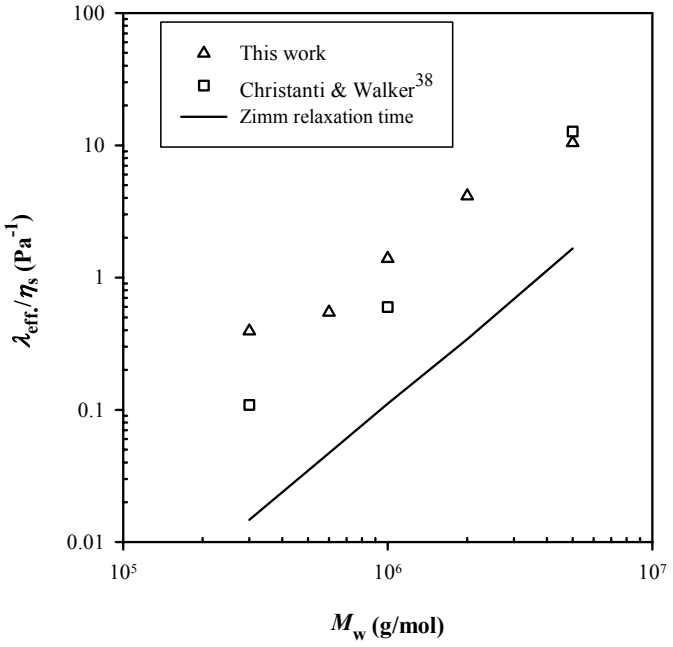

Figure 8 - Tirtaatmadja (Physics of Fluids)

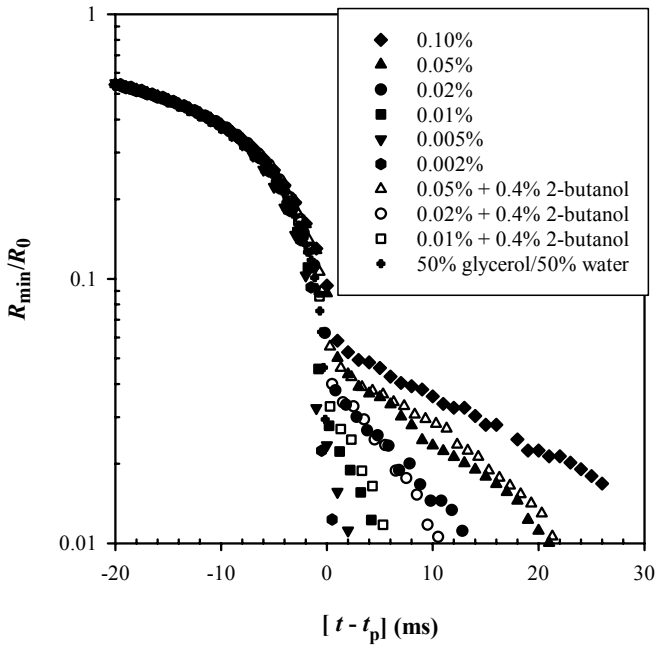

Figure 9 - Tirtaatmadja (Physics of Fluids)

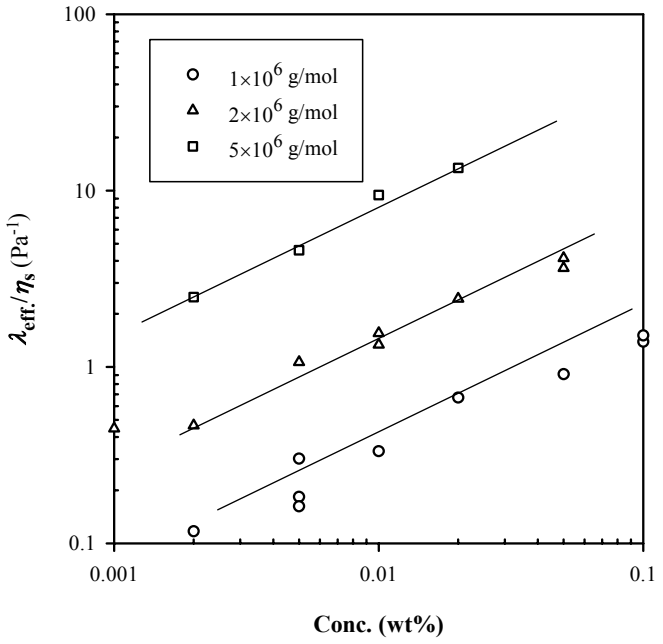

Figure 10 - Tirtaatmadja (Physics of Fluids)

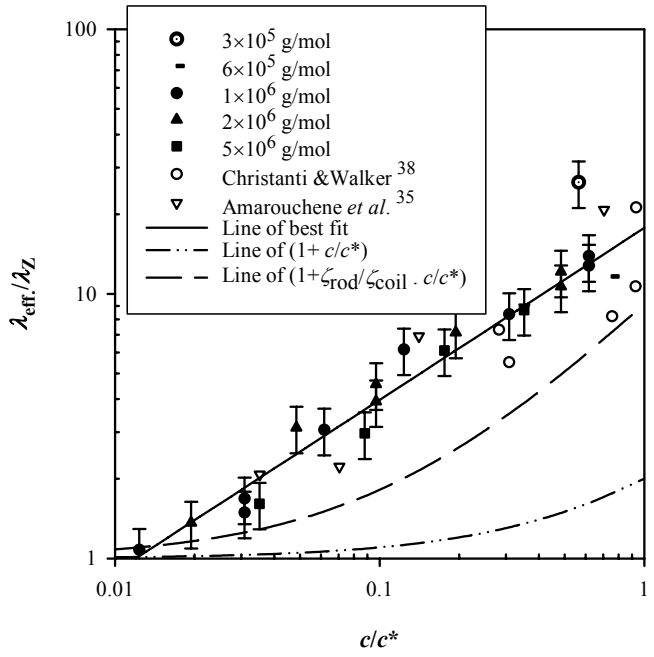

Figure 11 - Tirtaatmadja (Physics of Fluids)